

# Dynamical Linked Cluster Expansions: A Novel Expansion Scheme for Point-Link-Point-Interactions

Hildegard Meyer-Ortmanns\*

Institut für Theoretische Physik

Bergische Universität Wuppertal

Gaußstrasse 20

D-42097 Wuppertal, Germany

and

Thomas Reisz†

Institut für Theoretische Physik

Universität Heidelberg

Philosophenweg 16

D-69120 Heidelberg, Germany

December 5, 2017

## Abstract

Dynamical linked cluster expansions are linked cluster expansions with hopping parameter terms endowed with their own dynamics. This amounts to a generalization from 2-point to point-link-point interactions. We develop an associated graph theory with a generalized notion of connectivity and describe an algorithmic generation of the new multiple-line graphs. We indicate physical applications to spin glasses, partially annealed neural networks and  $SU(N)$  gauge Higgs systems. In particular the new expansion technique provides the possibility of avoiding the replica-trick in spin glasses. We consider variational estimates for the  $SU(2)$  Higgs model of the electroweak phase transition. The results for the transition line, obtained by dynamical linked cluster expansions, agree quite well with corresponding high precision Monte Carlo results.

---

\*E-mail address: ortmanns@theorie.physik.uni-wuppertal.de

†Supported by a Heisenberg Fellowship, E-mail address: reisz@thphys.uni-heidelberg.de

# 1 Introduction

Linked cluster expansions (LCEs) have a long tradition in statistical physics. Originally applied to classical fluids, later to magnetic systems ([1],[2],[3] and references therein), they were generalized to applications in particle physics in the eighties [4]. There they have been used to study the continuum limit of a lattice  $\Phi^4$  field theory in 4 dimensions at zero temperature. In [5, 6] they were further generalized to field theories at finite temperature, simultaneously the highest order in the expansion parameter was increased to 18. Usually the analytic expansions are obtained as graphical expansions. Because of the progress in computer facilities and the development of efficient algorithms for generating the graphs, it is nowadays possible to handle of the order of billions of graphs. The whole range from high temperatures down to the critical region becomes available, and thermodynamic quantities like critical indices and critical temperatures are determined with high precision (the precision is comparable or even better than in corresponding high quality Monte Carlo results) [6]-[9]. An extension of LCEs to a finite volume in combination with a high order in the expansion parameter turned out to be a particularly powerful tool for investigating the phase structure of systems with first and second order transitions by means of a finite size scaling analysis [10].

Linked cluster expansions are series expansions of the free energy and connected correlation functions about an ultralocal, decoupled theory in terms of a hopping parameter  $K$ . The corresponding graphical representation is a sum in terms of connected graphs. The value of  $K$  parametrizes the strength of interactions between fields at different lattice sites. Usually they are chosen as nearest neighbours, but also more general, less local couplings lead to convergent expansions ([11] and references therein) under appropriate conditions on the decay of the interactions. In contrast to the ultralocal terms of a generic interaction we will sometimes refer to hopping terms as non-ultralocal.

In this paper we develop dynamical linked cluster expansions (DLCEs). These are linked cluster expansions with hopping parameter terms that are endowed with their own dynamics. Such systems are realized in spin glasses or partially annealed neural networks with (fast) spins and (slow) interactions [12]-[14]. They also occur in variational estimates for  $SU(N)$ -gauge-Higgs systems as we will show later in this paper. Like LCEs they are expected to converge for a large class of interactions.

Formally DLCEs amount to a generalization of an expansion scheme from 2-point to point-link-point-interactions. These are interactions between fields associated with two points and with one pair of points called link. The points and links are not necessarily embedded on a lattice, and the links need not be restricted to nearest neighbours. We develop a new multiple-line graph theory in which a generalized notion of connectivity plays a central role. Standard notions of equivalence classes of graphs like 1-line irreducible and 1-vertex irreducible graphs have to be generalized, and new notions like 1-multiple-line irreducible graphs must be defined in order to give a systematic classification. We describe algorithms for generating these classes.

This is essential, since the number of graphs rapidly increases with the order in the expansion parameter. It typically exceeds the number of LCE-graphs by more than an order of magnitude.

The paper is organized as follows. In section 2 we specify the models that admit a DLCE. We introduce multiple-line graphs and explain the idea behind the abstract notions of multiple-line graph theory. Detailed definitions of multiple-line graphs, related notions and the computation of weights are given in section 3. Section 4 treats the issue of renormalization in the sense of suitable resummations of graphs. Algorithms for their generation are described in section 5. Applications to spin glasses and (partially annealed) neural networks are indicated in section 6. There it is of particular interest that DLCEs allow for the possibility of avoiding the replica trick. In section 7 we present results for the transition line of an SU(2) Higgs model. These are obtained by DLCEs applied to gap equations that follow from convexity estimates of the free energy density. The results are in good agreement with corresponding high precision Monte Carlo results [15]. Section 8 contains a summary and outlook.

The reader who is more interested in our actual applications of DLCEs may skip sections 3-5 in a first reading. These sections are of interest from a systematic point of view and essential if he is interested in applying DLCEs.

## 2 A Short Primer to DLCEs

In this section we first specify the class of models for which we develop dynamical linked cluster expansions. Next we illustrate some basic notions of multiple-line graph theory, in particular the need for a new notion of connectivity.

By  $\Lambda_0$  we denote a finite or infinite set of points. One of its realizations is a hypercubic lattice in  $D$  dimensions, infinite or finite in some directions with the topology of a torus.  $\Lambda_1$  denotes the set of unordered pairs  $(x, y)$  of sites  $x, y \in \Lambda_0$ ,  $x \neq y$ , also called unoriented links, and  $\bar{\Lambda}_1$  a subset of  $\Lambda_1$ .

We consider physical systems with a partition function of the generic form

$$\begin{aligned} Z(H, I, v) &\equiv \exp W(H, I, v) \\ &= \mathcal{N} \int \mathcal{D}\phi \mathcal{D}U \exp(-S(\phi, U, v)) \exp\left(\sum_{x \in \Lambda_0} H(x)\phi(x) + \sum_{l \in \bar{\Lambda}_1} I(l)U(l)\right), \end{aligned} \quad (1)$$

with measures

$$\mathcal{D}\phi = \prod_{x \in \Lambda_0} d\phi(x) \quad , \quad \mathcal{D}U = \prod_{l \in \bar{\Lambda}_1} dU(l) \quad (2)$$

and action

$$S(\phi, U, v) = \sum_{x \in \Lambda_0} S^0(\phi(x)) + \sum_{l \in \bar{\Lambda}_1} S^1(U(l)) - \frac{1}{2} \sum_{x, y \in \Lambda_0} v(x, y)\phi(x)U(x, y)\phi(y), \quad (3)$$

with non-ultralocal couplings

$$\begin{aligned}
v(x, y) &= v(y, x) \neq 0 && \text{only for } (x, y) \in \overline{\Lambda}_1, \\
&\text{in particular } v(x, x) = 0. && \tag{4}
\end{aligned}$$

For later convenience the normalization via  $\mathcal{N}$  is chosen such that  $W[0, 0, 0] = 0$ .

The field  $\phi(x)$  is associated with the sites  $x \in \Lambda_0$  and the field  $U(l)$  lives on the links  $l \in \overline{\Lambda}_1$ , and we write  $U(x, y) = U(l)$  for  $l = (x, y)$ . For definiteness and for simplicity of the notation here we assume  $\phi(x) \in \mathbf{R}$  and  $U(l) \in \mathbf{R}$ . In our actual applications  $\phi$  is a 4-component scalar field and  $U$  an  $SU(2)$ -valued gauge field, or  $\phi$  and  $U$  both are Ising spins, or the  $\phi$ s are the (fast) Ising spins and the  $U$ s  $\in \mathbf{R}$  the (slow) interactions. The action is split into two ultralocal parts,  $S^\circ$  depending on fields on single sites, and  $S^1$  depending on fields on single links  $l \in \overline{\Lambda}_1$ . For simplicity we choose  $S^1$  as the same function for all links  $l \in \overline{\Lambda}_1$ . We may identify  $\overline{\Lambda}_1$  with the support of  $v$ ,

$$\overline{\Lambda}_1 = \{l = (x, y) \mid v(x, y) \neq 0\}. \tag{5}$$

The support of  $v(x, y)$  need not be restricted to nearest neighbours, also the precise form of  $S^\circ$  and  $S^1$  does not matter for the generic description of DLCEs,  $S^\circ$  and  $S^1$  can be any polynomials in  $\phi$  and  $U$ , respectively. The only restriction is the existence of the partition function. In one of our applications  $S^\circ$  will be a  $\phi^4$ -type theory with  $O(N)$  symmetry,  $S^1$  consists of a term linear or quadratic in  $U$ .

Note that the interaction term  $v(x, y) \phi(x) U(x, y) \phi(y)$  contains a point-link-point-interaction and generalizes the 2-point-interactions  $v(x, y) \phi(x) \phi(y)$  of usual hopping parameter expansions. The effective coupling of the  $\phi$  fields has its own dynamics governed by  $S^1(U)$ , the reason why we have called our new expansion scheme *dynamical* LCE.

Dynamical linked cluster expansions are induced from a Taylor expansion of  $W(H, I, v) = \ln Z(H, I, v)$  about  $v = 0$ , the limit of a completely decoupled system. We want to express the series for  $W$  in terms of connected graphs. Let us consider the generating equation

$$\begin{aligned}
\partial W / \partial v(xy) &= 1/2 \langle \phi(x) U(x, y) \phi(y) \rangle \\
&= 1/2 \left( W_{H(x)I(x,y)H(y)} + W_{H(x)H(y)} W_{I(x,y)} \right. \\
&\quad + W_{H(x)I(x,y)} W_{H(y)} + W_{I(x,y)H(y)} W_{H(x)} \\
&\quad \left. + W_{H(x)} W_{H(y)} W_{I(x,y)} \right). \tag{6}
\end{aligned}$$

Here  $\langle \cdot \rangle$  denotes the normalized expectation value w.r.t. the partition function of Eq. (1). Subscripts  $H(x)$  and  $I(x, y) = I(y, x) = I(l)$  denote the derivatives of  $W$  w.r.t.  $H(x)$  and  $I(x, y)$ , respectively.

Next we would like to represent the right hand side of Eq. (6) in terms of connected graphs. Once we have such a representation for the first derivative of  $W$

w.r.t.  $v$ , graphical expansions for the higher derivatives can be traced back to the first one.

For each  $W$  in Eq. (6) we draw a shaded bubble, for each derivative w.r.t.  $H$  a solid line, called a  $\phi$ -line, with endpoint vertex  $x$ , and for each derivative w.r.t.  $I$  a dashed line, called a  $U$ -line, with link label  $l = (x, y)$ . The main graphical constituents are shown in Fig. 1. Two  $\phi$ -lines with endpoints  $x$  and  $y$  are then joined by means of a dashed  $U$ -line with label  $l$ , if the link  $l$  has  $x$  and  $y$  as its endpoints, i.e.  $l = (x, y)$ . According to these rules Eq. (6), multiplied by  $v(x, y)$  and summed over  $x$  and  $y$ , is represented by Fig. 2. Note that, because of the Taylor operation, each solid line from  $x$  to  $y$  carries a factor  $v(x, y)$ .

Since the actual need for a new type of connectivity is not quite obvious from Fig. 2, because Eq. (6) does not contain higher than first order derivatives w.r.t.  $I$ , let us consider a term

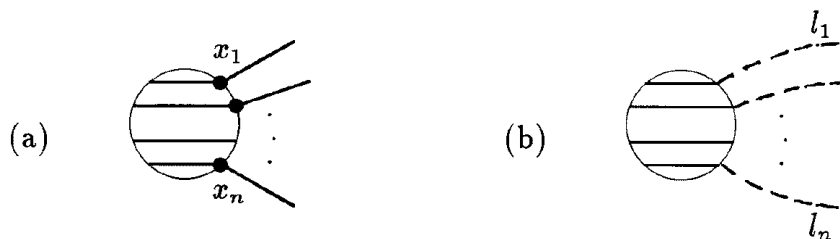


Figure 1: Graphical representation of the derivatives of  $W(H, I, v)$ . (a)  $n$ -point function  $\partial^n W / \partial H(x_1) \cdots \partial H(x_n)$ , (b)  $n$ -link function  $\partial^n W / \partial I(l_1) \cdots \partial I(l_n)$ .

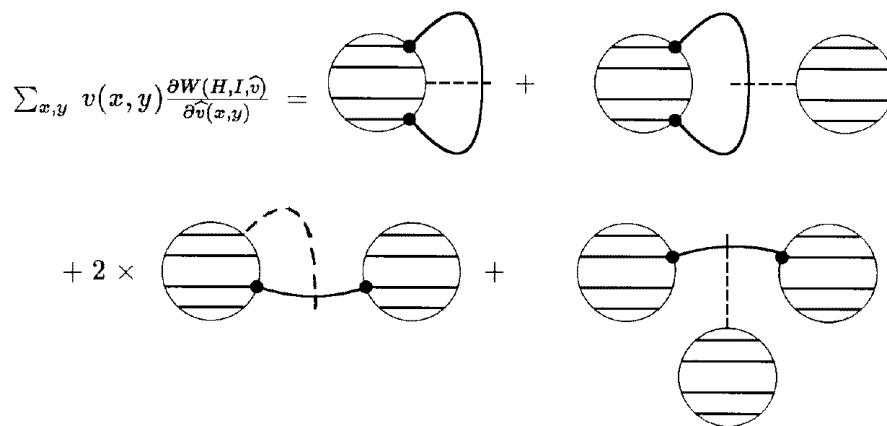


Figure 2: Generating equation of the graphical expansion of DLCEs. The solid line in each graph carries a propagator  $v(x, y)$ . A dashed  $U$ -line with label  $l$  intersects a solid line with endpoints  $x$  and  $y$  if  $l = (x, y)$ .

$$W_{H(x)} W_{H(y)} W_{H(r)} W_{H(s)} W_{I(x,y)I(r,s)} \quad (7)$$

occurring in the second derivative of  $W$  w.r.t.  $v(x, y), v(r, s)$ . According to the above rules this term would be represented as shown in Fig. 3a. While the 2 vertices in the last term of Fig. 2 are connected in the usual sense via a common (solid) line (the dashed line with an attached bubble could be omitted in this case), the graph in Fig. 3a would be disconnected in the old sense, since neither  $x$  nor  $y$  are line-connected with  $r$  and  $s$ , but -as a new feature of DLCE graphs- the lines from  $x$  to  $y$  and from  $r$  to  $s$  are connected via the dashed lines emerging from a common bubble shown in the middle of the graph. As we see from Fig. 3a, we need an additional notion of connectivity referring to the possibility of multiple-line connectivity. While the analytic expression is fixed, it is a matter of convenience to further simplify the graphical notation of Fig. 3a at  $v = 0$ . Two possibilities are shown in Fig. 3b and Fig. 3c. To Fig. 3b we later refer in the formal definition of the new type of multiple-line connectivity. In the familiar standard notion of connectivity two vertices of a graph are connected via lines. The vertices are line-connected. Already there, in a dual language, one could call two lines connected via vertices. The second formulation is just appropriate for our need to define when two lines are connected. The corresponding vertices mediating the connectivity of lines are visualized by tubes, in Fig. 3b we have just one of them. The tubes should be distinguished from the former type of vertices represented as full dots which are connected via bare  $\phi$ -lines. In Fig. 3c we show a simplified representation of Fig. 3b that we actually use in graphical expansions.

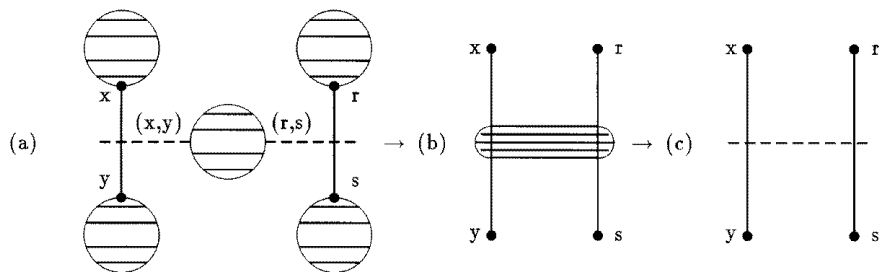


Figure 3: Representation of  $W_{H(x)}W_{H(y)}W_{H(r)}W_{H(s)}W_{I(x,y)I(r,s)}$ . (a) according to the rules of Fig. 1 and 2, (b) same as (a), but at  $v = 0$  and simplified for a formal definition of multiple-line connectivity, cf. section 3, (c) same as (b), but for use in the actual graphical representations.

The derivative terms have to be evaluated at  $v = 0$ . For  $v = 0$  we have a

decomposition of  $W$  according to

$$W(H, I, v = 0) = \sum_{x \in \Lambda_0} W^\circ(H(x)) + \sum_{l \in \bar{\Lambda}_1} W^1(I(l)) \quad (8)$$

with

$$\exp W^\circ(H) \equiv Z^\circ(H) = \frac{\int_{-\infty}^{\infty} d\phi \exp(-S^\circ(\phi) + H\phi)}{\int_{-\infty}^{\infty} d\phi \exp(-S^\circ(\phi))} \quad (9)$$

and

$$\exp W^1(l) \equiv Z^1(I) = \frac{\int_{-\infty}^{\infty} dU \exp(-S^1(U) + IU)}{\int_{-\infty}^{\infty} dU \exp(-S^1(U))}. \quad (10)$$

In Eq.s (9,10) we have omitted any single site or single link dependence, because we assume that  $S^\circ$  and  $S^1$  are the same for all  $x \in \Lambda_0$  and  $l \in \bar{\Lambda}_1$ , respectively. Therefore, at  $v = 0$ , the only non-vanishing derivatives of  $W$  are

$$W_{H(x_1)H(x_2)\dots H(x_n)} \Big|_{v=0} = \frac{\partial^n W^\circ(H(x_1))}{\partial H(x_1)^n} \cdot \delta_{x_1, x_2, \dots, x_n} \quad (11)$$

and

$$W_{I(l_1)I(l_2)\dots I(l_m)} \Big|_{v=0} = \frac{\partial^m W^1(I(l_1))}{\partial I(l_1)^m} \cdot \delta_{l_1, l_2, \dots, l_m}, \quad (12)$$

but mixed derivatives w.r.t.  $H$  and  $I$  vanish. As anticipated in Figs 3b and 3c, for  $v = 0$  we replace the dashed bubbles and graphically distinguish between bubbles with  $\phi$ -lines and bubbles with  $U$ -lines. We define

$$\left. \begin{array}{c} \text{---} \\ \text{---} \\ \vdots \\ \text{---} \end{array} \right\} n = v_n^{\circ c} = \left( \frac{\partial^n W^\circ(H)}{\partial H^n} \right)_{H=0} \quad (13)$$

for a connected  $n$ -point vertex with  $n \geq 1$  bare  $\phi$ -lines emerging from it and

$$\left. \begin{array}{c} \text{---} \\ \text{---} \\ \vdots \\ \text{---} \end{array} \right\} \nu = m_\nu^{1c} = \left( \frac{\partial^\nu W^1(I)}{\partial I^\nu} \right)_{I=0} \quad (14)$$

for a connected  $\nu$ -line consisting of  $\nu$  bare lines. If  $\nu = 1$ , we often omit the dashed line. If the bare lines of a  $\nu$ -line are internal  $\phi$ -lines, they get vertices attached to their endpoints, if they are external  $U$ -lines, no vertices will be attached.

Let  $V$  denote the lattice volume in  $D$  dimensions. The Taylor expansion of  $W$  about  $v = 0$  to second order in  $v$  then reads

$$\begin{aligned} W(H, I, v) &= W(H, I, v = 0) \\ &+ \sum_{x, y \in \Lambda_0} v(x, y) \frac{1}{2} W_{H(x)} W_{H(y)} W_{I(x, y)} \end{aligned}$$

$$\begin{aligned}
& + \frac{1}{2} \sum_{x,y,r,s \in \Lambda_0} \frac{1}{4} v(x,y)v(r,s) \\
& \cdot \left( \begin{aligned}
& 4 W_{H(y)} W_{H(s)} W_{H(r)H(x)} W_{I(x,y)} W_{I(r,s)} \\
& + 2 W_{H(x)H(r)} W_{H(y)H(s)} W_{I(x,y)} W_{I(r,s)} \\
& + 4 W_{H(y)} W_{H(s)} W_{H(r)H(x)} W_{I(x,y)I(r,s)} \\
& + 2 W_{H(r)H(x)} W_{H(y)H(s)} W_{I(r,y)I(x,s)} \\
& + W_{H(x)} W_{H(y)} W_{H(r)} W_{H(s)} W_{I(x,y)I(r,s)} \Big)_{v=0} \\
& + O(v^3),
\end{aligned} \right. \tag{15}
\end{aligned}$$

where we have used that  $v(x,x) = 0$ . For each  $W$  in the products of  $W$ s we now insert Eq.s (11),(12).

If we choose  $v$  in a standard way as next-neighbour couplings

$$v(x,y) = 2K \sum_{\mu=0}^{D-1} (\delta_{x+\hat{\mu},y} + \delta_{x-\hat{\mu},y}) \tag{16}$$

with  $\hat{\mu}$  denoting the unit vector in  $\mu$ -direction, Eq. (15) becomes in a graphical representation at  $H = I = 0$

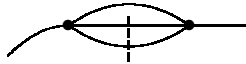
$$\begin{aligned}
\frac{W(0,0,v)}{V} &= (2K) \frac{1}{2} (2D) \bullet \text{---} \bullet \\
&+ (2K)^2 \left\{ \begin{aligned}
& \frac{1}{2} (2D)^2 \begin{array}{c} \bullet \\ \text{---} \\ \bullet \end{array} \quad + \frac{1}{4} (2D) \begin{array}{c} \bullet \\ \text{---} \\ \bullet \end{array} \\
& + \frac{1}{2} (2D)^2 \begin{array}{c} \bullet \\ \text{---} \\ \bullet \\ | \\ \bullet \end{array} \quad + \frac{1}{4} (2D) \begin{array}{c} \bullet \\ \text{---} \\ \bullet \\ | \\ \bullet \end{array} \\
& + \frac{1}{8} 2(2D) \begin{array}{c} \bullet \\ \text{---} \\ \bullet \\ | \\ \bullet \end{array} \quad \Big\} \\
&+ O(K^3).
\end{aligned} \tag{17}$$

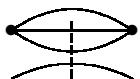
For clarity, here we have written explicitly the topological symmetry factors and the lattice embedding numbers. (Usually graphs represent their full weights including these factors.) Note that the first two graphs of the second order contribution also occur in a usual LCE with frozen  $U$ -dynamics, the next two differ by an additional dashed 2-line and the last one becomes even disconnected without the dashed line.

As usual, graphical expansions for correlation functions, in particular susceptibilities, are generated from  $W(H, I, v)$  by taking derivatives w.r.t. the external fields



$H$  and  $I$ . Graphically this amounts to attaching external  $\phi$ -lines and  $U$ -lines with

(1 endpoint) attached to vertices, e.g. 

(no endpoint) attached to  $\nu$ -lines, e.g.  (18)

In passing we remark that the conventional LCE is included as a special case of the DLCE, if the  $U$ -dynamics is "frozen" to some value  $U_0 \neq 0$ , so that

$$\begin{aligned} W^1(I) &= -S_1(U_0) + IU_0, \\ \frac{\partial W^1(I)}{\partial I} &= U_0, \\ \frac{\partial^n W^1(I)}{\partial I^n} &= 0 \quad \text{for all } n > 1, \end{aligned} \tag{19}$$

i.e., no  $n$ -lines do occur with  $n > 1$ . In this case it becomes redundant to attach dashed lines to bare lines. As mentioned above, in an LCE only the first three contributions would be left in Eq. (17).

### 3 Graphical expansion

#### 3.1 Multiple-line graph theory

The definition of a multiple-line graph as it will be given here is adapted to the computation of susceptibilities, where the sum is taken over all possible locations of the fields. The definition easily generalizes to correlation functions.

For details of the standard definition of graphs in the framework of linked cluster expansions and related notions we refer e.g. to [4, 5]. Here, for convenience, we briefly recall the very definition of a graph to point out the new properties of multiple-line graphs as defined below in this section.

A (standard LCE) graph or diagram is a structure

$$\tilde{\Gamma} = (\tilde{\mathcal{L}}_\Gamma, \tilde{\mathcal{B}}_\Gamma, \tilde{E}_\Gamma, \tilde{\Phi}_\Gamma), \tag{20}$$

where  $\tilde{\mathcal{L}}_\Gamma$  and  $\tilde{\mathcal{B}}_\Gamma \neq \emptyset$  are disjoint sets of internal lines and vertices of  $\tilde{\Gamma}$ , respectively.  $\tilde{E}_\Gamma$  is a map

$$\begin{aligned} \tilde{E}_\Gamma : \tilde{\mathcal{B}}_\Gamma &\rightarrow \{0, 1, 2, \dots\}, \\ v &\rightarrow \tilde{E}_\Gamma(v) \end{aligned} \tag{21}$$

that assigns to every vertex  $v$  the number of external lines  $\tilde{E}_\Gamma(v)$  attached to it. Finally,  $\tilde{\Phi}_\Gamma$  is the incidence relation that assigns internal lines to their two endpoints.

A multiple-line graph or multiple-line diagram is a structure

$$\Gamma = (\mathcal{L}_\Gamma, \mathcal{M}_\Gamma, \mathcal{B}_\Gamma, E_\Gamma^{(\phi)}, E_\Gamma^{(U)}, \Phi_\Gamma, \Psi_\Gamma). \quad (22)$$

$\mathcal{L}_\Gamma$ ,  $\mathcal{M}_\Gamma$  and  $\mathcal{B}_\Gamma$  are three mutually disjoint sets,

$$\mathcal{L}_\Gamma = \text{set of bare internal lines of } \Gamma, \quad (23)$$

$$\mathcal{M}_\Gamma = \text{set of multiple lines of } \Gamma, \quad (24)$$

$$\mathcal{B}_\Gamma = \text{set of vertices of } \Gamma. \quad (25)$$

$E_\Gamma^{(\phi)}$  is a map

$$\begin{aligned} E_\Gamma^{(\phi)} : \mathcal{B}_\Gamma &\rightarrow \{0, 1, 2, \dots\}, \\ v &\rightarrow E_\Gamma^{(\phi)}(v) \end{aligned} \quad (26)$$

that assigns to every vertex  $v$  the number of bare external  $\phi$ -lines  $E_\Gamma^{(\phi)}(v)$  attached to  $v$ . Every such  $\phi$ -line represents a field  $\phi$ . The number of external  $\phi$ -lines of  $\Gamma$  is denoted by  $E_\Gamma^{(\phi)} = \sum_{v \in \mathcal{B}_\Gamma} E_\Gamma^{(\phi)}(v)$ . Similarly,  $E_\Gamma^{(U)}$  is a map

$$\begin{aligned} E_\Gamma^{(U)} : \mathcal{M}_\Gamma &\rightarrow \{0, 1, 2, \dots\}, \\ m &\rightarrow E_\Gamma^{(U)}(m) \end{aligned} \quad (27)$$

that assigns to every multiple line  $m$  the number of external  $U$ -lines  $E_\Gamma^{(U)}(m)$  attached to  $m$ . Every such  $U$ -line represents a field  $U$  associated with a lattice link. The number of external  $U$ -lines of  $\Gamma$  is given by  $E_\Gamma^{(U)} = \sum_{m \in \mathcal{M}_\Gamma} E_\Gamma^{(U)}(m)$ .

Furthermore,  $\Phi_\Gamma$  and  $\Psi_\Gamma$  are incidence relations that assign bare internal lines to their endpoint vertices and to their multiple lines, respectively. We treat lines as unoriented. The generalization to oriented lines is easily done. More precisely, let  $\overline{(\mathcal{B}_\Gamma \times \mathcal{B}_\Gamma)'}'$  be the set of unordered pairs of vertices  $(v, w)$  with  $v, w \in \mathcal{B}_\Gamma$ ,  $v \neq w$ . (The bar implies unordered pairs, the prime the exclusions of  $(v, v)$ ,  $v \in \mathcal{B}_\Gamma$ .) As in the standard linked cluster expansion, self-lines are excluded. Every bare internal line is then mapped onto its pair of endpoints via

$$\Phi_\Gamma : \mathcal{L}_\Gamma \rightarrow \overline{(\mathcal{B}_\Gamma \times \mathcal{B}_\Gamma)'}'. \quad (28)$$

We say that  $v$  and  $w$  are the endpoint vertices of  $l \in \mathcal{L}_\Gamma$  if  $\Phi_\Gamma(l) = (v, w)$ . If there is such an  $l \in \mathcal{L}_\Gamma$ ,  $v$  and  $w$  are called neighbours. Similarly,  $\Psi_\Gamma$  is a map

$$\begin{aligned} \Psi_\Gamma : \mathcal{L}_\Gamma &\rightarrow \mathcal{M}_\Gamma, \\ l &\rightarrow \Psi_\Gamma(l) \end{aligned} \quad (29)$$

that maps every bare internal line to a multiple line. A multiple line  $m \in \mathcal{M}_\Gamma$  is composed of bare internal lines  $l \in \mathcal{L}_\Gamma$  which belong to  $m$  in the sense that  $\Psi_\Gamma(l) = m$ .  $l_{\mathcal{M}_\Gamma}(m)$  is the total number of bare internal lines belonging to  $m$ . With

$\nu = l_{\mathcal{M}_\Gamma}(m) + E_\Gamma^{(U)}(m)$ ,  $m$  is called a  $\nu$ -line. We always require that  $\nu \geq 1$ . On the other hand, every bare internal line belongs to one and only one multiple line. For simplicity we often identify a 1-line with the only one bare line that belongs to it.

Next we introduce some further notions that will be used later. External vertices are vertices having external  $\phi$ -lines attached,

$$\mathcal{B}_{\Gamma,ext} = \{v \in \mathcal{B}_\Gamma \mid E_\Gamma^{(\phi)}(v) \neq 0\}, \quad (30)$$

whereas internal vertices do not,  $\mathcal{B}_{\Gamma,int} = \mathcal{B}_\Gamma \setminus \mathcal{B}_{\Gamma,ext}$ . Similarly, external multiple lines have external  $U$ -lines attached,

$$\mathcal{M}_{\Gamma,ext} = \{m \in \mathcal{M}_\Gamma \mid E_\Gamma^{(U)}(m) \neq 0\}, \quad (31)$$

and the complement in  $\mathcal{M}_\Gamma$  are the internal multiple lines,  $\mathcal{M}_{\Gamma,int} = \mathcal{M}_\Gamma \setminus \mathcal{M}_{\Gamma,ext}$ .

For every pair of vertices  $v, w \in \mathcal{B}_\Gamma$ ,  $v \neq w$ , let  $\overline{\Phi}^1(v, w)$  be the set of lines with endpoint vertices  $v$  and  $w$ , and  $|\overline{\Phi}^1(v, w)|$  the number of these lines. Thus  $\overline{\Phi}^1(v, w)$  is the set of lines  $v$  and  $w$  have in common. With  $E_\Gamma^{(\phi)}(v)$  denoting the number of external  $\phi$ -lines attached to  $v \in \mathcal{B}_\Gamma$ ,

$$t_{\mathcal{B}_\Gamma}(v) = \sum_{w \in \mathcal{B}_\Gamma} |\overline{\Phi}^1(v, w)| + E_\Gamma^{(\phi)}(v) \quad (32)$$

is the total number of bare lines attached to  $v$ .

Some topological notions and global properties of graphs will be of major interest in the following. A central notion is the connectivity of a multiple-line graph. Recall that we want to consider the DLCE expansion of the free energy and of truncated correlation functions as an expansion in connected graphs. As indicated in section 2, the main generalization compared to the common notion of connectivity of a graph which is required here is that an additional type of connectivity is provided by multiple-lines. To define the connectivity of a multiple-line graph  $\Gamma$ ,  $\Gamma$  first is mapped to a (standard) LCE graph  $\overline{\Gamma}$  to which the standard notion of connectivity applies. There are various equivalent ways to define such a map. We choose the following one.

- For every multiple-line  $m \in \mathcal{M}_\Gamma$  define a new vertex  $w(m)$ . Let  $\tilde{\mathcal{B}}_\Gamma = \{w(m) \mid m \in \mathcal{M}_\Gamma\}$  and define  $\overline{\mathcal{B}} = \mathcal{B}_\Gamma \cup \tilde{\mathcal{B}}_\Gamma$  as the union of the vertices of  $\Gamma$  and the new set of vertices originating from the multiple-lines.
- For every bare internal line  $l \in \mathcal{L}_\Gamma$  define two new internal lines  $l_1, l_2$  and incidence relations

$$\begin{aligned} \overline{\Phi}(l_1) &= (v_1, w(\Psi_\Gamma(l))), \\ \overline{\Phi}(l_2) &= (v_2, w(\Psi_\Gamma(l))), \end{aligned} \quad (33)$$

where  $v_1$  and  $v_2$  are the two endpoint vertices of  $l$ . The set of all lines  $l_1, l_2$ , for all  $l \in \mathcal{L}_\Gamma$ , is denoted by  $\overline{\mathcal{L}}$ .

- Define the external incidence relations

$$\begin{aligned}
\bar{E} &: \bar{\mathcal{B}} \rightarrow \{0, 1, 2, \dots\}, \\
\bar{E}(v) &= E_{\Gamma}^{(\phi)}(v), \quad \text{for } v \in \mathcal{B}_{\Gamma}, \\
\bar{E}(v) &= E_{\Gamma}^{(U)}(m), \quad \text{for } v = w(m) \in \tilde{\mathcal{B}}_{\Gamma}.
\end{aligned} \tag{34}$$

Now,  $\bar{\Gamma}$  is defined by

$$\bar{\Gamma} = (\bar{\mathcal{L}}, \bar{\mathcal{B}}, \bar{E}, \bar{\Phi}). \tag{35}$$

Having defined the standard LCE graph  $\bar{\Gamma}$  for any multiple-line graph  $\Gamma$ , we call  $\Gamma$  multiple-line connected or just connected if  $\bar{\Gamma}$  is connected (in the usual sense). In Fig. 4 we have given two examples for a connected (upper graph) and a disconnected (lower graph) multiple-line graph .

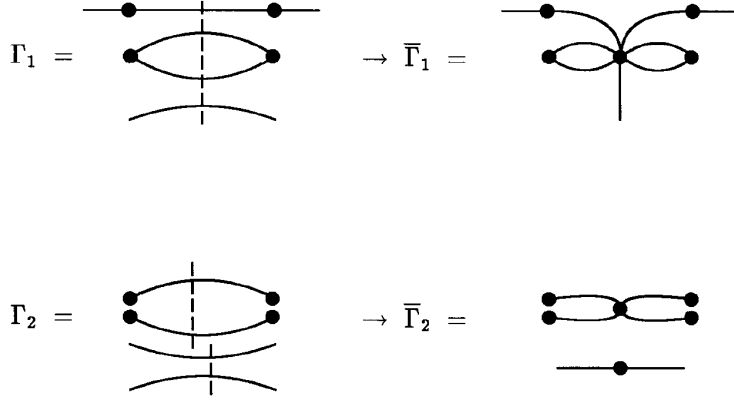


Figure 4: Example of multiple-line connectivity. The upper multiple-line graph  $\Gamma_1$  is connected because the graph  $\bar{\Gamma}_1$  is connected in the conventional sense. The lower multiple-line graph  $\Gamma_2$  is disconnected because  $\bar{\Gamma}_2$  is so.

The next important notion is the topological equivalence of two multiple-line graphs . Two multiple-line graphs

$$\Gamma_i = (\mathcal{L}_i, \mathcal{M}_i, \mathcal{B}_i, E_i^{(\phi)}, E_i^{(U)}, \Phi_i, \Psi_i), \quad i = 1, 2 \tag{36}$$

are called (topologically) equivalent if there are three invertible maps

$$\begin{aligned}
\phi_1 : \mathcal{B}_1 &\rightarrow \mathcal{B}_2, \\
\phi_2 : \mathcal{L}_1 &\rightarrow \mathcal{L}_2, \\
\phi_3 : \mathcal{M}_1 &\rightarrow \mathcal{M}_2,
\end{aligned} \tag{37}$$

such that

$$\begin{aligned}
\Phi_2 \circ \phi_2 &= \bar{\phi}_1 \circ \Phi_1, \\
\Psi_2 \circ \phi_2 &= \phi_3 \circ \Psi_1,
\end{aligned} \tag{38}$$

and

$$\begin{aligned} E_2^{(\phi)} \circ \phi_1 &= E_1^{(\phi)}, \\ E_2^{(U)} \circ \phi_3 &= E_1^{(U)}. \end{aligned} \quad (39)$$

Here  $\circ$  means decomposition of maps, and

$$\begin{aligned} \bar{\phi}_1 : \overline{\mathcal{B}_1 \times \mathcal{B}_1'} &\rightarrow \overline{\mathcal{B}_2 \times \mathcal{B}_2'} \\ \bar{\phi}_1(v, w) &= (\phi_1(v), \phi_1(w)). \end{aligned} \quad (40)$$

A symmetry of a multiple-line graph  $\Gamma = (\mathcal{L}, \mathcal{M}, \mathcal{B}, E^{(\phi)}, E^{(U)}, \Phi, \Psi)$  is a triple of maps  $\phi_1 : \mathcal{B} \rightarrow \mathcal{B}$ ,  $\phi_2 : \mathcal{L} \rightarrow \mathcal{L}$  and  $\phi_3 : \mathcal{M} \rightarrow \mathcal{M}$  such that

$$\begin{aligned} \Phi \circ \phi_2 &= \bar{\phi}_1 \circ \Phi, \\ \Psi \circ \phi_2 &= \phi_3 \circ \Psi, \end{aligned} \quad (41)$$

and

$$\begin{aligned} E^{(\phi)} \circ \phi_1 &= E^{(\phi)} \\ E^{(U)} \circ \phi_3 &= E^{(U)}. \end{aligned} \quad (42)$$

The number of these maps is called the symmetry number of  $\Gamma$ .

We denote by  $\mathcal{G}_{E_1, E_2}(L)$  the set of equivalence classes of connected multiple-line graphs with  $L$  bare internal lines,  $E_1$  external  $\phi$ -lines and  $E_2$  external  $U$ -lines. Furthermore we set

$$\mathcal{G}_{E_1, E_2} := \bigcup_{L \geq 0} \mathcal{G}_{E_1, E_2}(L). \quad (43)$$

A multiple line graph  $\Gamma$  does not need to have a vertex. If  $\mathcal{B}_\Gamma = 0$ , we have  $\mathcal{L}_\Gamma = 0$  as well. If in addition  $\Gamma$  is connected,  $\mathcal{M}_\Gamma$  consists of only one element, with all external  $U$ -lines attached to it. (We anticipate that  $\Gamma$  is 1-multiple-line irreducible (1MLI) by definition. For the definition of 1MLI cf. section 4 below.) The only graph of  $\mathcal{G}_{0, E}(L = 0)$  is given by

$$\Gamma = \left. \begin{array}{c} \text{---} \\ \text{---} \\ \vdots \\ \text{---} \\ \text{---} \end{array} \right\} E. \quad (44)$$

It represents the leading term of the susceptibility

$$\chi_{0, E} = \frac{1}{VD} \sum_{l_1, \dots, l_E \in \bar{\Lambda}_1} \langle U(l_1) \cdots U(l_E) \rangle^c \quad (45)$$

and is given by  $\partial^E W^1(I) / \partial I^E \big|_{I=0}$ . The index  $c$  in (45) stands for truncated (connected) correlation.

By removal of a  $\nu$ -line  $m \in \mathcal{M}_\Gamma$  we mean that  $m$  is dropped together with all bare internal lines and all external  $U$ -lines that belong to  $m$ . This notion is explained in Fig. 5a. (It is used in section 4 for 1-lines to define 1-particle irreducible (1PI) and 1-line irreducible (1LI) multiple-line graphs .)

On the other hand, by decomposition of a  $\nu$ -line  $m \in \mathcal{M}_\Gamma$  we mean that  $m$  is dropped together with the external  $U$ -lines of  $m$ , but all bare internal lines that belong to  $m$  are kept in the graph, being identified now with 1-lines. This notion will be used below to define 1MLI and renormalized multiple-line moments. It is illustrated in Fig. 5b.

Similarly, decomposition of a vertex  $v \in \mathcal{B}_\Gamma$  means to remove the vertex  $v$  and to attach the free end of every line that entered  $v$  before to a new vertex, a separate one for each line. This notion is used to define 1-vertex-irreducible (1VI) and renormalized vertex moments for multiple-line graphs . For an example see Fig. 5c.

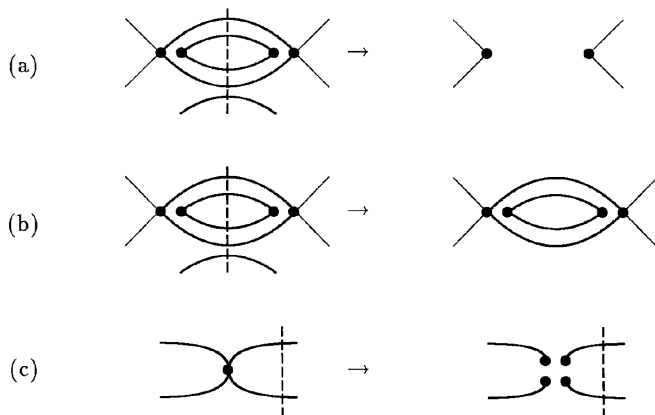


Figure 5: Removal (a) and decomposition (b) of a 5-line. Decomposition (c) of a vertex.

## 3.2 Susceptibilities and weights

In the last section we have defined multiple-line graphs and the notions of connectivity and equivalence of such graphs. The definition is chosen in such a way that the series expansions of the free energy and of truncated correlation functions are obtained as a sum over equivalence classes of connected multiple-line graphs . The number  $L$  of bare internal lines of a multiple-line graph  $\Gamma$  counts the order in the expansion parameter  $v(x, y)$  to which  $\Gamma$  contributes. If  $v(x, y)$  is of the form

$$v(x, y) = 2K \sum_{z \in \mathcal{N}(x)} \delta_{y,z}, \quad (46)$$

with  $\mathcal{N}(x)$  any finite  $x$ -dependent set of lattice sites, the contribution of  $\Gamma$  is a multiple of  $(2K)^L$ . Often used special cases are the nearest neighbour interactions

$$v(x, y) = 2K \sum_{\mu=0}^{D-1} (\delta_{x, y+\hat{\mu}} + \delta_{x, y-\hat{\mu}}) \quad (47)$$

and the uniform interaction

$$v(x, y) = 2K (1 - \delta_{x, y}), \quad (48)$$

which is used in models of spin glasses and partially annealed neural networks.

Susceptibilities of the  $\phi$  and  $U$  fields will be represented as

$$\begin{aligned} \chi_{E_1, E_2} &= \frac{1}{VD} \sum_{x_1, \dots, x_{E_1} \in \Lambda_0} \sum_{l_1, \dots, l_{E_2} \in \bar{\Lambda}_1} \langle \phi(x_1) \cdots \phi(x_{E_1}) U(l_1) \cdots U(l_{E_2}) \rangle^c \\ &\equiv \frac{1}{VD} \sum_{x_1, \dots, x_{E_1} \in \Lambda_0} \sum_{l_1, \dots, l_{E_2} \in \bar{\Lambda}_1} \left. \frac{\partial^{E_1+E_2} W(H, I, v)}{\partial H(x_1) \cdots \partial H(x_{E_1}) \partial I(l_1) \cdots \partial I(l_{E_2})} \right|_{H=I=0} \\ &= \sum_{L \geq 0} (2K)^L \sum_{\Gamma \in \mathcal{G}_{E_1, E_2}(L)} w(\Gamma) \end{aligned} \quad (49)$$

with lattice volume  $V$  and dimension  $D$ . Similar representations hold for higher moments  $\mu$ .

The weight  $w(\Gamma)$  of a multiple-line graph  $\Gamma \in \mathcal{G}_{E_1, E_2}(L)$  is given as the product of the following factors

- for every vertex  $v \in \mathcal{B}_\Gamma$  a factor

$$v_n^{\circ c} = \left( \frac{\partial^n W(H)}{\partial H^n} \right)_{H=0}, \quad (50)$$

where  $n = t_{\mathcal{B}_\Gamma}(v)$  is the total number of bare lines attached to  $v$ .

- for every multiple line  $m \in \mathcal{M}_\Gamma$  a factor

$$m_\nu^{1c} = \left( \frac{\partial^\nu W^1(I)}{\partial I^\nu} \right)_{I=0}, \quad (51)$$

where  $\nu = l_{\mathcal{M}_\Gamma}(m) + E_\Gamma^{(U)}(m)$ , that is  $m$  is a  $\nu$ -line,

- a factor  $1/S_\Gamma$ , where  $S_\Gamma$  is the topological symmetry number of  $\Gamma$ ,
- a factor counting the permutation symmetry of external  $\phi$ -lines,

$$\frac{E_\Gamma^{(\phi)}!}{\prod_{v \in \mathcal{B}_\Gamma} E_\Gamma^{(\phi)}(v)!}, \quad (52)$$

- a factor counting the permutation symmetry of external  $U$ -lines,

$$\frac{E_\Gamma^{(U)}!}{\prod_{m \in \mathcal{M}_\Gamma} E_\Gamma^{(U)}(m)!} \quad , \quad (53)$$

- the lattice embedding number of  $\Gamma$ , which is the number of ways  $\Gamma$  can be embedded on a lattice of given geometry, e. g. on a hypercubic lattice. To this end, the vertices of  $\Gamma$  (if any) are placed onto lattice sites. One arbitrary vertex is placed at a fixed lattice site, in order to account for the volume factor  $1/V$  in (49). A priori there is no exclusion principle. This means that any number of vertices can be placed at the same lattice site. (This is sometimes called free embedding.) Two restrictions apply to the embeddings. The first constraint results from the fact that a bare internal line represents a hopping propagator  $v(x, y)$ , with lattice sites  $x$  and  $y$  at which the two endpoint vertices of the line are placed at. A reasonable computation of the embedding number takes into account the particular form of  $v(x, y)$  from the very beginning. The second constraint is that bare lines of the same multiple-line have to be mapped on the same pair of sites.

For example, if  $v(x, y)$  is the nearest neighbour interaction (47), two vertices which have at least one line in common are to be placed at nearest neighbour lattice sites. On the other hand, a propagator  $v(x, y)$  of the form (48) implies a rather weak constraint in that  $x$  and  $y$  must be different, but otherwise can be freely placed over the lattice.

We remark that in case of a non-trivial internal symmetry (such as considered in section 7) the expressions of Eq.s (49)-(51) must be modified appropriately. In particular, the weight (51) of a multiple-line does no longer take such a simple form. Eq. (125) below is an example for the case of a hopping term originating in an SU(2) Higgs model.

## 4 Renormalization

Truncated correlation functions, susceptibilities and other moments are obtained as sums over multiple-line graphs that are connected. Their number rapidly grows with increasing order, that is with increasing number of bare internal lines. The procedure of "renormalization" means that the connected moments are represented in terms of reduced ones. The reduced moments are obtained by summation over multiple-line graph classes which are more restricted than just by their property of being connected. Of course the number of graphs of such classes is smaller. Only the most restricted multiple-line graph classes must be constructed. The subsequent steps towards the moment computation are most conveniently done by operating analytically with the reduced moments. In particular, it is no longer necessary



to generate all connected and the corresponding intermediate multiple-line graph classes.

A connected multiple-line graph  $\Gamma$  is called 1-particle irreducible (1PI) if it satisfies the following condition. Remove an arbitrary 1-line of  $\Gamma$ . There is at most one connected component left that has external lines attached. (This notion is the same as the one used in the context of Feynman graphs.) On the other hand, if in addition the remaining graph is still connected, then  $\Gamma$  is called 1-line irreducible (1LI). In many cases it is sufficient to use only the second notion. It is for instance sufficient that all vertices are constrained to have only an even number of lines attached, or more generally, if graphs and subgraphs with one external line are forbidden. For notational simplicity we assume in the following that this is the case and henceforth refer only to the notion 1LI <sup>1</sup>. The generalization to the case in which 1LI and 1PI graphs must be distinguished goes along the same lines as for LCEs, which was discussed in [16].

By  $\mathcal{G}_{E_1, E_2}^{1LI}(L)$  we denote the subset of multiple-line graphs  $\Gamma \in \mathcal{G}_{E_1, E_2}(L)$  that are 1LI. 1LI-susceptibilities are defined as series in the hopping parameter similarly as in (49) by restricting the summation to 1LI graphs,

$$\chi_{E_1, E_2}^{1LI} = \sum_{L \geq 0} (2K)^L \sum_{\Gamma \in \mathcal{G}_{E_1, E_2}^{1LI}(L)} w(\Gamma). \quad (54)$$

Susceptibilities are easily obtained in a closed form in terms of 1LI-susceptibilities  $\chi^{1LI}$ . It can be shown that the  $\chi^{1LI}$ s can be obtained by an appropriate Legendre transform. For instance

$$\begin{aligned} \chi_{2,0} &= \frac{\chi_{2,0}^{1LI}}{1 - \tilde{v}(0)\chi_{2,0}^{1LI}}, \\ \chi_{2,1} &= \frac{\chi_{2,1}^{1LI}}{(1 - \tilde{v}(0)\chi_{2,0}^{1LI})^2}, \end{aligned} \quad (55)$$

where  $\tilde{v}(k)$  is the Fourier transform of the hopping propagator  $v(x, y)$ ,

$$v(x, y) = \int_{-\pi}^{\pi} \frac{d^D k}{(2\pi)^D} e^{-ik \cdot (x-y)} \tilde{v}(k). \quad (56)$$

In LCEs the second important resummation comes from so called vertex renormalizations. This means partial resummation of graphs with specific properties such as having one external vertex only. These sums then are considered as "renormalized vertices" replacing the vertices of graphs with complementary properties. The procedure naturally leads to the notion of 1-vertex irreducibility (1VI) and renormalized moments.

In DLCE we follow this procedure. The very definition of 1VI has to be modified slightly for multiple-line graphs because of the enhanced connectivity properties due

---

<sup>1</sup>In ref. [4, 5] the term 1PI was used instead.

to multiple-lines. In addition, as a natural generalization, we supplement vertex renormalization by multiple-line renormalization.

A multiple-line graph  $\Gamma$  is called 1-vertex irreducible (1VI) if it satisfies the following condition. Decompose an arbitrary vertex  $v \in \mathcal{B}_\Gamma$ . Every connected component of the remaining graph has then at least one external line attached. It can be a  $\phi$ -line or a  $U$ -line. We write

$$\mathcal{G}_{E_1, E_2}^{1VI}(L) = \{\Gamma \in \mathcal{G}_{E_1, E_2}^{1LI}(L) \mid \Gamma \text{ is 1VI}\} \quad (57)$$

for the set of equivalence classes of graphs that are both 1LI and 1VI, with  $E_1$  external  $\phi$ -lines,  $E_2$  external  $U$ -lines and  $L$  bare internal lines.

The renormalized vertex moment graphs are 1LI graphs that have precisely one external vertex and no external multiple line,

$$Q_k(L) = \{\Gamma \in \mathcal{G}_{k,0}^{1LI}(L) \mid \text{there is } v \in \mathcal{B}_\Gamma \text{ with } E_\Gamma^{(\phi)}(v) = k\}. \quad (58)$$

A multiple-line graph  $\Gamma$  is called 1-multiple-line irreducible (1MLI) if it satisfies the following criterion. Decompose an arbitrary multiple-line  $m \in \mathcal{M}_\Gamma$ . Every remaining connected component has then at least one external line attached. It can be a  $\phi$ -line or a  $U$ -line. We write

$$\mathcal{G}_{E_1, E_2}^{1MLI}(L) = \{\Gamma \in \mathcal{G}_{E_1, E_2}^{1LI}(L) \mid \Gamma \text{ is 1MLI}\}. \quad (59)$$

The renormalized multiple-line moment graphs are graphs that are 1LI and have precisely one external multiple-line, but no external vertex,

$$R_k(L) = \{\Gamma \in \mathcal{G}_{0,k}^{1LI}(L) \mid \text{there is } m \in \mathcal{M}_\Gamma \text{ with } E_\Gamma^{(U)}(m) = k\}. \quad (60)$$

The equivalence classes of graphs that are both 1VI and 1MLI are denoted by

$$S_{E_1, E_2}(L) = \mathcal{G}_{E_1, E_2}^{1VI}(L) \cap \mathcal{G}_{E_1, E_2}^{1MLI}(L). \quad (61)$$

With the renormalized moment graphs as defined above, the 1LI-susceptibilities are now obtained in the form

$$\chi_{E_1, E_2}^{1LI} = \sum_{L \geq 0} (2K)^L \sum_{\Gamma \in S_{E_1, E_2}(L)} \tilde{w}(\Gamma). \quad (62)$$

The weights  $\tilde{w}(\Gamma)$  are given as a product of factors as described in the last subsection, with the following two exceptions.

- The vertex coupling constants  $v_n^{\text{oc}}$  are replaced by the renormalized vertex moments

$$v_n^{\text{oc}} \rightarrow v_n^c = \sum_{L \geq 0} (2K)^L \sum_{\Gamma \in Q_n(L)} w(\Gamma). \quad (63)$$

- The multiple line coupling constants  $m_\nu^{1c}$  are replaced by the renormalized multiple line moments

$$m_\nu^{1c} \rightarrow m_\nu^c = \sum_{L \geq 0} (2K)^L \sum_{\Gamma \in \mathcal{R}_\nu(L)} w(\Gamma). \quad (64)$$

In the series representations above, the  $w(\Gamma)$  are computed according to the rules of subsection 3.2.

## 5 Graph construction

In this section we describe a mechanism to generate the multiple-line graph classes  $\mathcal{S}_{E_1, E_2}(L)$ ,  $\mathcal{Q}_k(L)$  and  $\mathcal{R}_k(L)$  with  $L \geq 1$  internal lines. Similar as in LCEs the idea is to define appropriate classes of vacuum graphs (no external lines). The generation of the graphs of  $\mathcal{S}$ ,  $\mathcal{Q}$  and  $\mathcal{R}$  is then done by attaching external lines in various ways. By defining appropriate recursion relations, the order by order construction can then be restricted to the vacuum classes.

Fortunately we can profit from graphs that have been generated already in standard LCEs. This way we completely avoid a cumbersome recursive construction, but obtain the vacuum multiple-line graphs by operating on the LCE vacuum graphs of the same order.

The graphs of  $\mathcal{S}$ ,  $\mathcal{Q}$  and  $\mathcal{R}$  will be obtained through a sequence of simpler graph classes. At each step, any method of multiple-line graph construction should satisfy the following two conditions.

- It should be surjective or complete. At least one graph of every equivalence class should be generated.
- For every equivalence class precisely one representant should be kept. All generated graphs of a particular class of graphs should be mutually inequivalent. This requires a so called non-equivalence test for every newly generated graph. The graph should be kept if and only if it is not equivalent to a graph already generated. In general it must be compared with all multiple-line graphs that have been generated before. If this is necessary, the non-equivalence test is rather time consuming.

The algorithm we describe below circumvents an extensive comparison of multiple-line graphs. It is defined in such a way that two graphs can be equivalent only if they have their origin in the same graph of the prior graph class.

Essentially we proceed in the following steps. The starting point are the vacuum diagrams of  $\mathcal{P}_2(L)$  as computed in [5].  $\mathcal{P}_2(L)$  is the set of (standard) LCE equivalence classes of connected, 1LI vacuum graphs with  $L$  lines. Operating on

$\mathcal{P}_2(L)$ , we generate all mutually inequivalent multiple-line graphs with  $L$  lines that are connected, 1LI and have no external lines (neither  $\phi$ -lines nor  $U$ -lines),

$$\mathcal{MP}_2(L) \equiv \mathcal{G}_{0,0}^{1LI}(L). \quad (65)$$

This is done in two steps. In a first step lines with the same endpoint vertices are arranged in all possible ways into multiple lines. We obtain a subset of  $\mathcal{MP}_2(L)$  which we denote by  $\widetilde{\mathcal{MP}}_2(L)$ . A multiple-line graph  $\Gamma \in \mathcal{MP}_2(L)$  belongs to  $\widetilde{\mathcal{MP}}_2(L)$ ,  $\Gamma \in \widetilde{\mathcal{MP}}_2(L)$ , if and only if all bare lines of  $\Gamma$  that belong to the same multiple line have the same endpoint vertices. The second step is to relax the additional constraint on  $\widetilde{\mathcal{MP}}_2(L)$ . This is achieved by resolving the vertices. This means that every vertex is split into several ones, and that the bare lines that were attached to the original vertex before now are distributed over the new vertices in all possible ways. As a general constraint on the resolutions, the resulting multiple-line graphs should be 1LI in order to stay in  $\mathcal{MP}_2(L)$ . We impose an additional constraint on the resolutions, allowing only for so-called admissible vertex resolutions. They are defined in such a way that two multiple-line graphs of  $\mathcal{MP}_2(L)$  can be equivalent only if they originate from the same graph of  $\widetilde{\mathcal{MP}}_2(L)$ . This considerably simplifies the non-equivalence test.

Once we have obtained  $\mathcal{MP}_2(L)$ , the final multiple-line graph classes  $\mathcal{S}_{E_1, E_2}(L)$ ,  $\mathcal{Q}_k(L)$  and  $\mathcal{R}_k(L)$  are obtained by attaching external  $\phi$ -lines and  $U$ -lines in the appropriate way to all graphs of  $\mathcal{MP}_2(L)$ . The steps in the generation of the DLCE graph classes are shown schematically in Fig. 6.

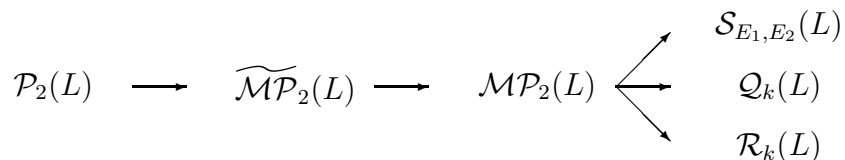


Figure 6: Modules in the generation of DLCE graph classes. The root of the inheritance tree are the LCE vacuum graphs of  $\mathcal{P}_2(L)$ . By means of multiple-line construction ( $\widetilde{\mathcal{MP}}_2$ ) and vertex resolution ( $\mathcal{MP}_2$ ) the DLCE vacuum graphs of  $\mathcal{MP}_2(L)$  are obtained. Attaching external  $\phi$ -lines and external  $U$ -lines in well defined ways yields the renormalized vertices ( $\mathcal{Q}_k(L)$ ), the multiple-line moments ( $\mathcal{R}_k(L)$ ), and the 1MLI and 1VI graphs ( $\mathcal{S}_{E_1, E_2}(L)$ ).

In the following we describe the multiple-line graph construction in detail. Below we use the following notation. For any finite set  $\mathcal{A}$  let  $\mathcal{P}(\mathcal{A})$  denote the set of partitions of  $\mathcal{A}$  into mutually disjoint nonempty subsets of  $\mathcal{A}$ . For every  $\Pi \in \mathcal{P}(\mathcal{A})$  we have

$$\mathcal{A} = \bigcup_{P \in \Pi} P. \quad (66)$$

### 5.1 $\mathcal{P}_2(L) \rightarrow \widetilde{\mathcal{MP}}_2(L)$

Starting with the LCE vacuum graphs of  $\mathcal{P}_2(L)$ , we first of all arrange internal lines into multiple lines. Consider an arbitrary graph  $\Gamma \in \mathcal{P}_2(L)$ . Simultaneously for every pair of neighbouring vertices  $v, w \in \mathcal{B}_\Gamma$  choose a partition  $\Pi \in \mathcal{P}(\mathcal{L}_{v,w})$ , where  $\mathcal{L}_{v,w}$  is the set of common lines between the vertices  $v$  and  $w$ . Every  $l \in \mathcal{L}_{v,w}$  belongs to a unique  $P \in \Pi \in \mathcal{P}(\mathcal{L}_{v,w})$ . For every  $P \in \Pi$  we introduce a multiple line  $m(P)$  such that all  $l \in P$  are precisely the bare internal lines that belong to  $m(P)$ . This procedure defines the incidence relation  $\Psi(l)$  for all  $l \in \mathcal{L}_\Gamma$  and, along with that, a multiple-line graph that belongs to  $\widetilde{\mathcal{MP}}_2(L)$ .

In Fig. 7 we give examples for this construction. In the first one, an LCE graph leads to 5 mutually inequivalent DLCE graphs, in the second one to 3 DLCE graphs of  $\widetilde{\mathcal{MP}}_2(L)$ .

Proceeding this way for all partitions of lines for all pairs of neighbored vertices of  $\Gamma$ , and for all  $\Gamma \in \mathcal{P}_2(L)$ , we obtain the class of multiple-line graphs  $\widetilde{\mathcal{MP}}_2(L)$ . The non-equivalence check for every newly generated multiple-line graph  $\tilde{\Gamma}$  can be drastically restricted. It is sufficient to compare  $\tilde{\Gamma}$  only with those multiple-line graphs that have been constructed before from the same graph  $\Gamma \in \mathcal{P}_2(L)$  as  $\tilde{\Gamma}$  results from. Other graphs of  $\widetilde{\mathcal{MP}}_2(L)$  are inequivalent to  $\tilde{\Gamma}$ .

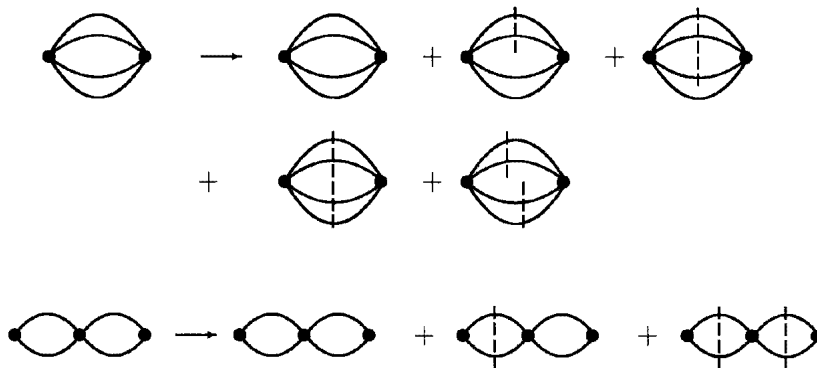


Figure 7: Two examples of multiple-line construction  $\mathcal{P}_2(L) \rightarrow \widetilde{\mathcal{MP}}_2(L)$  with  $L = 4$ . Common lines between two vertices are arranged into multiple lines in all possible ways. Only mutually inequivalent graphs are shown.

### 5.2 $\widetilde{\mathcal{MP}}_2(L) \rightarrow \mathcal{MP}_2(L)$

The second step is to relax the constraint on  $\widetilde{\mathcal{MP}}_2$  that bare lines which belong to the same multiple line must have the same endpoint vertices. This is achieved by

vertex resolutions of all graphs of  $\widetilde{\mathcal{MP}}_2(L)$ . To efficiently reduce the non-equivalence check of new graphs we allow only for so-called admissible vertex resolutions.

Let  $\tilde{\Gamma} \in \widetilde{\mathcal{MP}}_2(L)$ ,  $v \in \mathcal{B}_{\tilde{\Gamma}}$  any vertex of  $\tilde{\Gamma}$  and  $\Pi \in \mathcal{P}(\mathcal{L}_v)$  any partition of the set of lines  $\mathcal{L}_v$  entering  $v$ . We remove the vertex  $v$  and draw for every  $P \in \Pi$  a new vertex  $v(P)$  so that all lines  $l \in P$  enter the vertex  $v(P)$  rather than  $v$  before its removal. This procedure is called a vertex resolution of  $v$ . The resulting graph  $\Gamma$  must be 1LI in order to belong to  $\mathcal{MP}_2(L)$ .

The vertex resolution of  $v$  is called admissible if in addition the (standard LCE) graph  $\hat{\Gamma}$  is connected with  $\hat{\Gamma}$  defined in the following way. For every  $l \in \mathcal{L}_v$  there is precisely one  $m \in \mathcal{M}_{\tilde{\Gamma}}$  with  $\Psi_{\tilde{\Gamma}}(l) = m$ , and there is exactly one  $P \in \Pi$  with  $l \in P$ . Draw a vertex  $w(m) = w(\Psi_{\tilde{\Gamma}}(l))$  for every such multiple line, a vertex  $v(P)$  for every  $P \in \Pi$ , and define a line  $\hat{l}(l)$  with incidence relation

$$\hat{\Phi}(\hat{l}) = (w(\Psi_{\tilde{\Gamma}}(l)), v(P)). \quad (67)$$

This defines a graph  $\hat{\Gamma} = (\mathcal{B}_{\hat{\Gamma}}, \mathcal{L}_{\hat{\Gamma}}, E_{\hat{\Gamma}} = 0, \hat{\Phi})$  with

$$\begin{aligned} \mathcal{B}_{\hat{\Gamma}} &= \{v(P) | P \in \Pi\} \cup \{w(\Psi_{\tilde{\Gamma}}(l)) | l \in \mathcal{L}_v\} \\ \mathcal{L}_{\hat{\Gamma}} &= \{\hat{l}(l) | l \in \mathcal{L}_v\}. \end{aligned} \quad (68)$$

A vertex resolution is called admissible if the graph  $\hat{\Gamma}$  is connected. Roughly speaking this implies that no vertex drops off after vertex resolution.

Fig. 8 shows two admissible and one non-admissible vertex resolutions (the auxiliary graphs  $\hat{\Gamma}$  are not displayed).

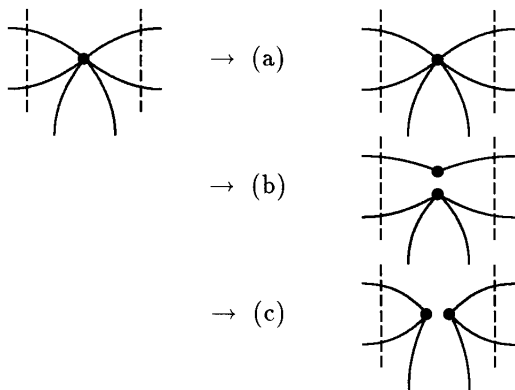


Figure 8: Example of admissible ((a) and (b)) and non-admissible (c) vertex resolutions. In particular, the case of the trivial resolution (a) is admissible.

The class  $\mathcal{MP}_2(L)$  is now generated as follows. Consider an arbitrary graph  $\tilde{\Gamma} \in \widetilde{\mathcal{MP}}_2(L)$ . Simultaneously for all vertices  $v \in \mathcal{B}_{\tilde{\Gamma}}$  apply an admissible vertex

resolution. We obtain a multiple-line graph  $\Gamma \in \mathcal{MP}_2(L)$ . Doing this for all possible resolutions of all vertices and for all  $\tilde{\Gamma} \in \widetilde{\mathcal{MP}}_2(L)$ , we get the complete graph class  $\mathcal{MP}_2(L)$ . Again, due to the restriction to admissible vertex resolutions, the non-equivalence check of a newly generated graph  $\Gamma \in \mathcal{MP}_2(L)$  can be restricted to graphs that have been generated from the same graph of  $\widetilde{\mathcal{MP}}_2(L)$  as  $\Gamma$  was.

In Fig. 9 we show an example for the application of admissible vertex resolutions. Here one graph of  $\widetilde{\mathcal{MP}}_2(L)$  leads to eight graphs of  $\mathcal{MP}_2(L)$ , indicating the proliferation of DLCE graphs. Note that the starting graph was only one of five of Fig. 7.

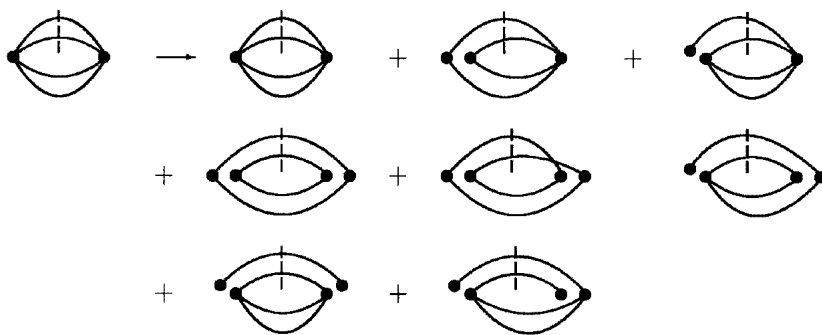


Figure 9: Example of applying admissible vertex resolutions for  $\widetilde{\mathcal{MP}}_2(L) \rightarrow \mathcal{MP}_2(L)$  with  $L = 4$ . Only mutually inequivalent graphs are shown.

### 5.3 $\mathcal{MP}_2(L) \rightarrow \mathcal{S}_{E_1, E_2}(L)$ , $Q_k(L)$ and $R_k(L)$

The final step is to construct the classes of multiple-line graphs  $\mathcal{S}_{E_1, E_2}$ ,  $Q_k$  and  $R_k$  out of the vacuum multiple-line graphs of  $\mathcal{MP}_2$ . This step is realized by attaching external  $\phi$ -lines and external  $U$ -lines in different ways to every multiple-line graph  $\Gamma \in \mathcal{MP}_2(L)$ .

$R_k(L)$  is obtained by attaching  $k$  external  $U$ -lines to just one multiple line  $m \in \mathcal{M}_\Gamma$ , for all multiple lines  $m$  and for all  $\Gamma$ .

$Q_k(L)$  is obtained by attaching  $k$  external  $\phi$ -lines to just one vertex  $v \in \mathcal{B}_\Gamma$ , for all vertices  $v$  and for all  $\Gamma$ .

$\mathcal{S}_{E_1, E_2}(L)$  is obtained by attaching  $E_1$  external  $\phi$ -lines to the vertices of  $\Gamma$  and  $E_2$  external  $U$ -lines to the multiple lines of  $\Gamma$ , for all  $\Gamma \in \mathcal{MP}_2(L)$ . This is done under the constraint that the resulting multiple-line graphs have to be 1VI and 1MLI.

Again, the non-equivalence test of multiple-line graphs can be confined to pairs of graphs that have their origin in the same graph of  $\mathcal{MP}_2(L)$ .

In Fig. 10 we illustrate the attachment of external lines to a vacuum DLCE graph of  $\mathcal{MP}_2(L)$ .

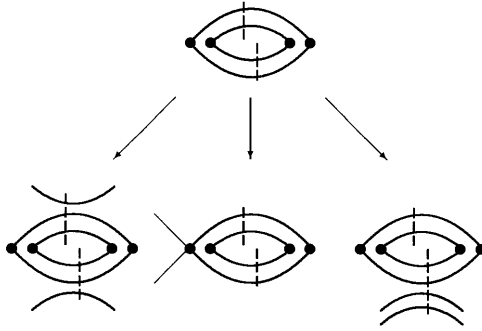


Figure 10: Attaching external lines to a vacuum DLCE graph of  $\mathcal{MP}_2(L)$ . The example shows from left to right: the generation of a graph of  $\mathcal{S}_{0,2}(L)$ ,  $Q_2(L)$  and  $R_2(L)$ , with  $L = 4$ .

## 6 Applications to Spin Glasses and Neural Networks

In this section we indicate applications of DLCEs to spin glasses and partially annealed neural networks with "slow" interactions and "fast" spins [12]-[14], [17].

### 6.1 The SK model and the replica trick

For simplicity we consider the Sherrington-Kirkpatrick (SK) model which is a spin glass model with infinite connectivity [12]. Following the notation of section 2, the fast spins are represented by the  $\Phi$ -field  $\Phi_i$ ,  $i = 1, \dots, N$ , taking values in  $\{-1, +1\}$ .  $N$  denotes the total number of spins. The slow interactions are mediated by the  $U$ -field  $U_{(i,j)}$ ,  $i < j = 1, \dots, N$ . The SK model is described by the partition function

$$Z'_{\beta'} = \mathcal{N} \int_{-\infty}^{\infty} \prod_{i < j=1}^N dU_{(i,j)} \exp(-\beta' \mathcal{H}(U)), \quad (69)$$

with  $\mathcal{N}$  some normalization that will be specified below. The effective Hamiltonian  $\mathcal{H}$  of  $U$  is given by

$$\mathcal{H}(U) = -\frac{1}{\beta} \ln Z_{\beta}(U) + \frac{1}{2} \mu N \sum_{i < j=1}^N U_{(i,j)}^2, \quad (70)$$

where  $\mu$  is a positive coupling constant.  $Z_{\beta}(U)$  is the partition function of a spin system

$$Z_{\beta}(U) = \sum_{\{\Phi_i = \pm 1\}} \exp\left(\beta \sum_{i < j} U_{(i,j)} \Phi_i \Phi_j\right) \quad (71)$$



at frozen spin-spin couplings  $U_{(i,j)}$  and temperature  $\beta^{-1}$ , controlling the fast spin fluctuations. In (69) it has been assumed that the equilibrium distribution of the slow variables is a Boltzmann distribution governed by a second temperature  $\beta'^{-1}$ . This assumption is justified, if the time evolution of the  $U$ s is determined by a dissipative Langevin equation (for the precise conditions see e.g. [18]). Such a Langevin equation can be actually derived for the  $U$ s from an ansatz which is motivated by neural networks [12]-[14].

One of the major quantities of interest is  $\ln Z'_{\beta'}$ . Let us first rewrite  $Z'_{\beta'}$  in the form

$$\begin{aligned} Z'_{n\beta} &= \int_{-\infty}^{\infty} \prod_{i<j=1}^N \left( \sqrt{\frac{JN}{2\pi}} dU_{(i,j)} \right) \cdot \exp\left(-\frac{1}{2}JN \sum_{i<j} U_{(i,j)}^2\right) Z_{\beta}(U)^n \\ &\equiv [[Z_{\beta}(U)^n]], \end{aligned} \quad (72)$$

where we have introduced  $J = \beta\mu$  and  $n = \beta'/\beta$ . The normalization has been chosen such that  $[[1]] = 1$ .

The limiting case  $n = 0$  with  $J$  kept fixed corresponds to a quenching of the  $U$ s in a spin glass, in this limit the  $U$  degrees of freedom decouple from the spin dynamics, while  $n = 1$  corresponds to a pure annealing in the disordered system (see e.g. [13]). Partial annealing then refers to a value of  $n$  with  $0 < n < 1$ . In particular the limit  $n \rightarrow 0$  with fixed  $J$  and  $\beta$  amounts to the replica trick in spin glasses [18]. Assuming that averaging  $[[\cdot]]$  and limes  $n \rightarrow 0$  commute, we have

$$[[\ln Z_{\beta}(U)]] = \lim_{n \rightarrow 0} \frac{\ln Z'_{n\beta}}{n}. \quad (73)$$

The left hand side of (73) is calculated by means of the right hand side.

So far  $n$  has been a positive real number. For integer  $n = 1, 2, \dots$ ,  $Z_{\beta}(U)^n$  is the partition function of an  $n$ -times replicated system. Let us first consider this case. We rewrite

$$Z_{\beta}(U)^n = \sum_{\{\Phi_i^{(a)}\}} \exp\left(\beta \sum_{a=1}^n \sum_{i<j=1}^N U_{(i,j)} \Phi_i^{(a)} \Phi_j^{(a)}\right), \quad (74)$$

with  $a = 1, \dots, n$  labelling the replicated spin variables, so that

$$\begin{aligned} Z'_{n\beta} &= \int_{-\infty}^{\infty} \prod_{i<j=1}^N dU_{(i,j)} \cdot \sum_{\{\Phi_i^{(a)} = \pm 1\}} \exp(-S(U, \Phi^{(a)})), \\ S(U, \Phi^{(a)}) &= -\beta \sum_{a=1}^n \sum_{i<j=1}^N U_{(i,j)} \Phi_i^{(a)} \Phi_j^{(a)} + \frac{1}{2}JN \sum_{i<j} U_{(i,j)}^2. \end{aligned} \quad (75)$$

Linear terms in  $\Phi$  and  $U$  may be included according to

$$S_{lin} = -h \sum_{a=1}^n \sum_{i=1}^N \Phi_i^{(a)} + c \sum_{i<j=1}^N U_{(i,j)} \quad (76)$$

with constant external fields  $h$  and  $c$ . Apparently  $Z'_{n\beta}$  has the form of models to which DLCE applies, with a hopping term

$$S_{hop}(U, \Phi^{(a)}) = -\beta \sum_{a=1}^n \sum_{i < j=1}^N U_{(i,j)} \Phi_i^{(a)} \Phi_j^{(a)}, \quad (77)$$

a single link action

$$S^1(U_{(i,j)}) = cU_{(i,j)} + \frac{1}{2}JN U_{(i,j)}^2, \quad (78)$$

and a single site action

$$S^o(\Phi_i^{(a)}) = -h \sum_{a=1}^n \Phi_i^{(a)}. \quad (79)$$

Application of DLCE to  $\ln Z'_{\beta'}$  and derived quantities yields their series expansions in  $\beta$ .

So far, merely for simplicity, we have considered the SK model which is a spin glass model with infinite and uniform connectivity, in which all spins are coupled with equal variance  $[[U_{(i,j)}^2]] = 1/(JN)$ . For integer  $n = 1, 2, \dots$ , this system becomes exactly solvable in the thermodynamic limit corresponding to the limit  $N \rightarrow \infty$ , so that the leading order of a large- $N$  expansion becomes exact, cf. e.g. [17]. In DLCE this amounts to a resummation of appropriate tree graphs.

In cases of finite or non-uniform connectivity it is no longer possible to obtain solutions in a closed form. Examples are multilayered neural networks with couplings between adjacent layers, and spin glasses with short range interactions. Models of this kind are suited for an application of DLCEs and will be studied in future work.

Finally we come to the limiting case of  $n = 0$ . Usually it is obtained by extrapolating the results obtained for  $n = 1, 2, \dots$  towards  $n = 0$ . For instance,  $[[\ln Z_{\beta}(U)]]$  is obtained from  $[[Z_{\beta}(U)^n]]$  for  $n = 1, 2, \dots$ . This is a rather subtle point because the extrapolation is not unique without further assumptions. In the next subsection we show how it is possible to completely avoid both the extrapolation and the replica trick and to directly compute the quantity of interest by means of dynamical linked cluster expansions. The task is to appropriately identify the classes of contributing graphs.

## 6.2 Avoiding the replica trick

First we adapt the notation to section 2 to include more general cases.  $\Lambda_0$  denotes the support of the spins, that is the set of lattice sites, with  $V = |\Lambda_0|$  denoting their total number.  $\bar{\Lambda}_1 \subseteq \Lambda_1$  are the pairs of sites whose spins interact. In accordance with (72), we write for the normalized link-average of a function  $f(U)$

$$[[f(U)]] = \int \mathcal{D}U f(U) \quad (80)$$

with

$$\begin{aligned} \mathcal{D}U &= \prod_{l \in \bar{\Lambda}_1} d\mu(U(l)), \\ d\mu(U) &= \mathcal{N}_1 dU \exp(-S^1(U)), \quad \int_{-\infty}^{\infty} d\mu(U) = 1. \end{aligned} \quad (81)$$

It is convenient to introduce the single link expectation values

$$\langle g(U) \rangle_1 \equiv \int d\mu(U) g(U) \quad (82)$$

and the generating function  $W^1(I)$  by

$$\exp W^1(I) \equiv \langle \exp(IU) \rangle_1. \quad (83)$$

The way in which the replica trick can be avoided is exemplified for the free energy density  $W_{sp}/V$  of the spin system averaged over the link couplings. The partition function of the spin system for a given distribution of the link interactions  $U(x, y)$  is given by

$$\exp W_{sp}(U) = \mathcal{N}_{sp} \int \mathcal{D}\Phi \exp(-S_{sp}(\Phi, U)), \quad (84)$$

where  $W_{sp}(0) = 0$  and

$$\begin{aligned} S_{sp}(\Phi, U) &= -\frac{1}{2} \sum_{x, y \in \Lambda_0} v(x, y) \Phi(x) \Phi(y) U(x, y), \\ \mathcal{D}\Phi &= \prod_{x \in \Lambda_0} d\Phi(x) \cdot \exp(-S^\circ(\Phi(x))). \end{aligned} \quad (85)$$

Without loss of generality we identify the support of the interaction  $v(x, y) = v(y, x)$  with the set  $\bar{\Lambda}_1$  of lattice sites where  $\mathcal{D}U$  is supported,

$$\bar{\Lambda}_1 = \{l = (x, y) \in \overline{\Lambda_0 \times \Lambda_0} \mid v(x, y) \neq 0\}. \quad (86)$$

For simplicity we assume  $v(x, y)$  to be of the form (46), so that  $K$  is a measure of the strength of the interactions  $v(x, y)$ .

The free energy density of the spin system allows for a series expansion in the standard LCE sense, with the link field  $U(l)$  playing the role of a "background field",

$$\frac{1}{V} W_{sp}(U) = \sum_{L \geq 0} (2K)^L \sum_{\Gamma \in \mathcal{G}_0^{sp}(L)} w^{sp}(\Gamma, U). \quad (87)$$

Here  $\mathcal{G}_E^{sp}(L)$  (with  $E = 0$ ) denotes the set of equivalence classes of connected LCE graphs with  $E$  external lines and  $L$  internal lines. The spin-weights  $w^{sp}(\Gamma, U)$  are of the form

$$w^{sp}(\Gamma, U) = R^{sp}(\Gamma) \sum_{\mathcal{L}_\Gamma \rightarrow \bar{\Lambda}_1} \prod_{l \in \bar{\Lambda}_1} U(l)^{m(l)}. \quad (88)$$

The sum is taken over all non-vanishing lattice embeddings of the graph  $\Gamma$ . It runs over all maps of internal lines of the graph  $\Gamma$  to pairs of lattice sites of  $\bar{\Lambda}_1$  that are consistent with the graph topology in the sense discussed in section 3. For every  $l \in \bar{\Lambda}_1$ ,  $m(l)$  denotes the number of lines of  $\Gamma$  that are mapped onto the link  $l$  by the embedding. All other factors that contribute to the weight are collected in the prefactor  $R^{sp}(\Gamma)$ , including the inverse topological symmetry number of  $\Gamma$ .

Next we want to express  $[[W_{sp}(U)]]$  as a series in  $K$  by means of DLCE. Toward this end we set  $f(U) = W_{sp}(U)$  and insert the series (87) with (88) into (80). At this stage we are not concerned with question of (uniform or dominated) convergence and obtain

$$\begin{aligned} \left[ \left[ \frac{1}{V} W_{sp}(U) \right] \right] &= \sum_{L \geq 0} (2K)^L \sum_{\Gamma \in \mathcal{G}_0^{sp}(L)} \int \mathcal{D}U w^{sp}(\Gamma, U) \\ &= \sum_{L \geq 0} (2K)^L \sum_{\Gamma \in \mathcal{G}_0^{sp}(L)} R^{sp}(\Gamma) \sum_{\mathcal{L}_\Gamma \rightarrow \bar{\Lambda}_1} \prod_{l \in \bar{\Lambda}_1} \langle U(l)^{m(l)} \rangle_1. \end{aligned} \quad (89)$$

The next step is to express the full single link expectation values in terms of the connected ones. They are related by

$$\langle U^m \rangle_1 = \sum_{\Pi \in \mathcal{P}(\underline{m})} \prod_{P \in \Pi} \langle U^{|P|} \rangle_1^c, \quad (90)$$

where  $\mathcal{P}(\underline{m})$  denotes the set of all partitions of  $\underline{m} = \{1, \dots, m\}$  into non-empty, mutually disjoint subsets of  $\underline{m}$ .  $|P|$  is the number of elements of the set  $P$ . The relation (90) is equivalent to the partition of all lines of  $\Gamma$  that are mapped to the same lattice link into multiple lines, with every multiple line contributing a factor

$$\langle U^{|P|} \rangle_1^c = \left. \frac{\partial^{|P|} W^1(I)}{\partial I^{|P|}} \right|_{I=0} = m_{|P|}^{1c}. \quad (91)$$

Using (90), (91) we rewrite (89) as

$$\left[ \left[ \frac{1}{V} W_{sp}(U) \right] \right] = \sum_{L \geq 0} (2K)^L \sum_{\Gamma \in \mathcal{G}_0^{sp}(L)} R^{sp}(\Gamma) \sum_{\Pi \in \mathcal{P}(\mathcal{L}_\Gamma)} \left( \prod_{P \in \Pi} m_{|P|}^{1c} \right) \left( \sum_{\Pi \rightarrow \bar{\Lambda}_1} \prod_{l \in \bar{\Lambda}_1} 1 \right). \quad (92)$$

The last summation in (92) is over all maps  $\mathcal{L}_\Gamma \rightarrow \bar{\Lambda}_1$  of the lines of  $\Gamma$  to the lattice links of  $\bar{\Lambda}_1$  subject to the constraint that all lines that belong to the same multiple-line corresponding to some  $P \in \Pi$  are mapped onto the same lattice link.

Finally we rewrite (92) as a sum over multiple-line graphs. To this end, we first observe that for every  $\Gamma \in \mathcal{G}_0^{sp}(L)$ , every partition  $\Pi \in \mathcal{P}(\mathcal{L}_\Gamma)$  of the lines of  $\Gamma$  into multiple-lines generates a multiple-line graph  $\Delta = (\Gamma, \Pi)$  in the obvious way. Let us denote by  $\overline{\mathcal{G}}_{0,0}(L)$  the subset of multiple-line graphs of  $\mathcal{G}_{0,0}(L)$  that stay connected after decomposition of all multiple lines. (These are the multiple-line graphs which stay connected in the usual graph theoretical sense, when the dashed lines are omitted.) For every  $\Delta \in \overline{\mathcal{G}}_{0,0}(L)$  there is a unique  $\Gamma(\Delta) \in \mathcal{G}_0^{sp}(L)$  and at least one  $\Pi \in \mathcal{P}(\mathcal{L}_{\Gamma(\Delta)})$  such that  $(\Gamma(\Delta), \Pi) = \Delta$ . Let  $n_\Delta$  be the (uniquely determined) number of partitions  $\Pi \in \mathcal{P}(\mathcal{L}_{\Gamma(\Delta)})$  with  $(\Gamma(\Delta), \Pi) = \Delta$ , and  $\Pi(\Delta)$  such an arbitrary partition. Eq. (92) then becomes

$$\left[ \left[ \frac{1}{V} W_{sp}(U) \right] \right] = \sum_{L \geq 0} (2K)^L \sum_{\Delta \in \overline{\mathcal{G}}_{0,0}(L)} n_\Delta R^{sp}(\Gamma(\Delta)) \left( \prod_{P \in \Pi(\Delta)} m_{|P|}^{1c} \right) \left( \sum'_{\Pi(\Delta) \rightarrow \overline{\Lambda}_1} 1 \right). \quad (93)$$

The last bracket of (93) is the lattice embedding factor of the multiple-line graph  $\Delta$ . The second bracket from the right does not depend on the choice of  $\Pi(\Delta)$  and is the product of the multiple-line coupling constants as defined in section 3. Finally,  $n_\Delta R^{sp}(\Gamma(\Delta))$  is precisely the remaining part of the weight of  $\Delta$  that was described in detail in section 3, endowed with the correct inverse topological symmetry number of the multiple-line graph  $\Delta$  (because of the factor  $n_\Delta$ ).

In summary, we obtain the series expansion of the link-averaged free energy density in terms of DLCE graphs,

$$\left[ \left[ \frac{1}{V} W_{sp}(U) \right] \right] = \sum_{L \geq 0} (2K)^L \sum_{\Delta \in \overline{\mathcal{G}}_{0,0}(L)} w(\Delta). \quad (94)$$

The weight  $w(\Delta)$  of a multiple-line graph  $\Delta$  is defined and computed according to the rules given in section 3.

Eq. (94) is the series representation of the link-averaged free energy density of the spin system, i.e. the free energy density of the  $n = 0$  replica system, in terms of DLCE graphs. It looks much like the series representation of the 1-replica system, which is given by

$$\frac{1}{V} W_{1-repl} \equiv \frac{1}{V} \ln [\exp W_{sp}(U)] = \sum_{L \geq 0} (2K)^L \sum_{\Delta \in \mathcal{G}_{0,0}(L)} w(\Delta) \quad (95)$$

according to the discussion of section 2. We recall that  $\mathcal{G}_{0,0}(L)$  is the set of DLCE vacuum graphs with  $L$  bare lines that are connected in the generalized DLCE sense. Comparing (94) and (95), the transition from  $n = 1$  to  $n = 0$  replicas is achieved by keeping only the subset  $\overline{\mathcal{G}}_{0,0}(L) \subseteq \mathcal{G}_{0,0}(L)$  of multiple-line graphs that are connected in the original (LCE) sense.

We expect that the series (94) are convergent for a large class of interactions  $S^1(U)$  and  $v(x, y)$  if the coupling constant  $K$  is sufficiently small. For special interactions most of the multiple-line graphs yield vanishing contributions so that we

can further restrict the sum to a subset of  $\overline{\mathcal{G}}_{0,0}(L)$ . An example is given by the mean field type of interaction of the SK model where all pairs of sites are coupled with the same strength. That is, in the notation of this subsection,

$$\begin{aligned} v(x, y) &= K(1 - \delta_{x,y}), \\ \overline{\Lambda}_1 &\equiv \Lambda_1 \text{ is the set of all pairs of sites,} \\ S^1(U) &= V \frac{1}{2} U^2. \end{aligned} \tag{96}$$

In the thermodynamic limit  $V \rightarrow \infty$  only those multiple-line graphs survive that consist exclusively of 2-lines, and that do not contain any loop of 2-lines. The resulting tree structure provides the possibility of summing the series (94) and of analytically continuing the result to the spin glass phase of large coupling  $K$ . Work in this direction is in progress.

## 7 Applications to the SU(2) Higgs model

In this section we discuss applications of DLCEs to study the Higgs transition within a variational estimate for the gauged SU(2) Higgs model. The estimate serves as an effective description of the electroweak standard model.

We consider a 4-dimensional hypercubic finite temperature lattice  $\Lambda_0$  of size  $L_0 \times V_3$ , with  $L_0 = T^{-1}$  the inverse temperature in lattice units and  $V_3$  the spatial volume. The lattice links are the set of nearest neighbour lattice sites, given by

$$\overline{\Lambda}_1 = \{(x; \mu) \mid x \in \Lambda_0, \mu = 0, \dots, 3\}. \tag{97}$$

The gauge field  $U(x; \mu)$  is an SU(2) valued field living on the lattice links  $\overline{\Lambda}_1$ . It is convenient to parametrize such an SU(2) matrix by

$$\begin{aligned} U &= \phi_0(U) \mathbf{1}_2 + i \vec{\sigma} \cdot \vec{\phi}(U) \\ &\equiv U_0 + i \vec{\sigma} \cdot \vec{U} \end{aligned} \tag{98}$$

with  $U \simeq (U_0, \vec{U}) \in S_3$ . The Higgs field  $\Phi$  lives on the lattice sites  $\Lambda_0$ . Its values are real multiples of SU(2),

$$\begin{aligned} \Phi(x) &= \phi_0(\Phi(x)) \mathbf{1}_2 + i \vec{\sigma} \cdot \vec{\phi}(\Phi(x)) \\ &\equiv \phi_0(x) + i \vec{\sigma} \cdot \vec{\phi}(x), \end{aligned} \tag{99}$$

with  $\phi \simeq (\phi_0(x), \vec{\phi}(x)) \in \mathbf{R}^4$ . We say that  $\Phi$  is  $cU(2)$  valued.

As a special case of Eq. (1) we consider the partition function

$$Z_{VE1} = \int \mathcal{D}U \mathcal{D}\Phi \exp(-S_{VE1}(U, \Phi)), \tag{100}$$

in which

$$\mathcal{D}U = \prod_{x \in \Lambda_0} \prod_{\mu=0}^3 d\mu_H(U(x; \mu)), \quad (101)$$

with  $d\mu_H(U)$  the normalized Haar measure on  $SU(2)$ , and

$$\mathcal{D}\Phi = \prod_{x \in \Lambda_0} \exp(-S^\circ(\Phi(x))) d\nu(\Phi(x)), \quad (102)$$

where

$$\begin{aligned} d\nu(\Phi) &= d^4\phi, \\ S^\circ(\Phi) &= \frac{1}{2} \text{tr}(\Phi^\dagger \Phi) + \lambda \left( \frac{1}{2} \text{tr}(\Phi^\dagger \Phi) - 1 \right)^2 \\ &= \phi^2 + \lambda (\phi^2 - 1)^2. \end{aligned} \quad (103)$$

Finally,

$$\begin{aligned} S_{VE1}(U, \Phi) &= - \sum_{x \in \Lambda_0} \left\{ 4\zeta_{link} \phi_0(U(x; 0)) + \sum_{\mu=1}^3 4\zeta_{cube} \phi_0(U(x; \mu)) \right. \\ &\quad + \sum_{\mu=1}^3 (2\kappa) \frac{1}{2} \text{tr}(\Phi(x)^\dagger U(x; \mu) \Phi(x + \hat{\mu})) \\ &\quad \left. + \xi \phi_0(\Phi(x)) \right\}, \end{aligned} \quad (104)$$

depending on variational parameters  $\zeta_{link}$ ,  $\zeta_{cube}$  and  $\xi \in \mathbf{R}$ , and on the hopping parameter  $\kappa$ . The first two terms are non-gauge invariant substitutes for the Wilson plaquette term of the gauge part of the  $SU(2)$  Higgs model, cf. Eq. (106) below. We distinguish timelike from spacelike directions. Timelike links are denoted as  $(x; 0)$  and spacelike as  $(x; \mu)$ ,  $\mu = 1, 2, 3$ . The third term is a hopping term coupling  $\Phi$  and  $U$  fields only in spatial directions. The last term depends on the third variational parameter  $\xi$  associated with the Higgs field  $\Phi$ , while the remaining ultralocal action for  $\Phi$  has been absorbed in the measure.

In the next subsection we first indicate how we arrive at the action (104) within a variational estimate for the free energy of the  $SU(2)$  Higgs model. We derive equations for the optimal choice of variational parameters and an equation -based on stability arguments- to determine the critical hopping parameter  $\kappa_{crit}$  at which the Higgs phase transition sets in. These equations will depend on expectation values of n-point correlations that are most suitably evaluated with a DLCE in three dimensions.

The generic graphical expansion exposed in sections 3-5 now has to be adapted to account for the internal symmetry. This is somewhat involved so that we restrict our discussion to some remarks in section 7.2, but postpone any details to a forthcoming paper [19]. In section 7.3 we present some results for the critical line in comparison with other variational estimates and Monte Carlo simulations.

## 7.1 Variational estimates for the free energy of the SU(2) Higgs model

By means of DLCEs we want to obtain an analytic estimate for the critical line in the SU(2) Higgs model that serves as an effective description of the Higgs transition in the electroweak standard model. Because of the rather different methodical ansatz in this approach, for a common choice of parameters this estimate will provide an independent check of numerical results based on Monte Carlo simulations. In addition, larger scalar field couplings are available in our approach and larger values for  $L_0$ , the number of time slices. (In our calculations  $L_0 = 4$  or  $L_0 = \infty$ , while it was chosen as 2 or 3 in [15].) Larger  $L_0$ s are required for a finite size scaling control.

To fix the notation we introduce the action of the SU(2) Higgs model as

$$\begin{aligned} Z &= \int \mathcal{D}U \mathcal{D}\Phi \exp(-S(U, \Phi)), \\ S(U, \Phi) &= S_W(U) + S_{hop}, \\ S_{hop} &= - \sum_{x \in \Lambda_0} \left\{ \sum_{\mu=0}^3 (2\kappa) \frac{1}{2} \text{tr} (\Phi(x)^\dagger U(x; \mu) \Phi(x + \hat{\mu})) \right\}. \end{aligned} \quad (105)$$

The Higgs self-interaction has been absorbed in the measure  $\mathcal{D}\Phi$  of Eq. (102),  $S_{hop}$  is the hopping parameter term in 4 dimensions.  $S_W$  is the SU(2) gauge invariant Wilson action

$$S_W(U) = \sum_{x \in \Lambda_0} \sum_{\mu < \nu = 0}^3 \bar{\beta} \left( 1 - \frac{1}{2} \text{Re tr} U(x; \mu) U(x + \hat{\mu}; \nu) U(x + \hat{\nu}; \mu)^{-1} U(x; \nu)^{-1} \right) \quad (106)$$

with gauge coupling  $\bar{\beta} \equiv 4/g^2$  and  $U \in SU(2)$  as in (104).

A plaquette term involves a 4-link interaction. In contrast to the hopping parameter term it does not allow for a direct treatment with DLCEs. Therefore we replace  $Z$ , the full partition function of the SU(2) Higgs model, by a partition function  $Z_{VE}$  that is related to  $Z$  by an inequality of the form

$$\exp(-Vf) \equiv Z \geq Z_{VE} \exp(< -(S - S_{VE}(\zeta)) >_{VE}) \equiv \exp(-V\tilde{f}(\zeta)). \quad (107)$$

Eq. (107) follows from the convexity of the exponential function and holds independently of the specific choice of  $Z$  and  $Z_{VE}$ , if the measure is positive definite and normalized.  $V$  is the 4-dimensional volume,  $f$  denotes the true physical free energy density defined via  $Z$ ,  $\tilde{f}$  the trial free energy density defined via the second equality in (107).  $S$  refers to the original action in  $Z$ , in our case it is the SU(2) Higgs action, and  $S_{VE}$  to an ansatz for the action in  $Z_{VE}$  depending on a generic set of variational parameters  $\zeta$ . These parameters should be optimized so that the difference of the trial and the physical free energy density  $\tilde{f}(\zeta) - f \geq 0$  becomes minimal for  $\zeta = \tilde{\zeta}$  at which  $\tilde{f}$  takes its minimum.



The most naive ansatz for  $S_{VE}$  is a mean field ansatz in the spirit of a molecular field approximation, leading to a factorization of  $Z_{VE0}$  according to

$$Z_{VE0}(\zeta, \xi) = Z_{link}^{4L_0V_3}(\zeta) \cdot Z_{site}^{L_0V_3}(\xi). \quad (108)$$

The partition function depends on two variational parameters  $\zeta$  and  $\xi$  and factorizes in a product over single link ( $Z_{link}$ ) and single site ( $Z_{site}$ ) partition functions,  $V_3$  denotes the three-dimensional volume. In this ansatz there is no space for implementing an asymmetry between temporal and spatial directions. Thus the results will be temperature independent by construction.

One can think of a variety of improvements of the molecular field ansatz, arguments against or in favour of the various versions will be given in [19]. Here we only consider the ansatz which is most plausible from a physical point of view and leads to the best agreement with Monte Carlo results for comparable sets of parameters. The ansatz treats the spacelike degrees of freedom of the hopping term in 3 dimensions beyond the mean field level (that is with DLCE), but the timelike degrees of freedom within a mean field approach, so that the partition function factorizes over the spacelike hyperplanes. The reason is that the spatial hopping term is supposed to contain the nonperturbative properties of the full model that drive the Higgs phase transition. While a mean field approach for all variables will be too rough to produce high quality results for  $\kappa_{crit}$ , it appears more reasonable for timelike variables, although a finite temperature effect on the Higgs transition gets lost this way. (We should remark that from results in a scalar  $\Phi^4$  theory in four dimensions the finite temperature effect on  $\kappa_{crit}$  is expected to be anyway quite small [4, 6].)

Now it is easily checked that the choice of  $S_{VE1}$  in Eq. (104) leads to a factorization of  $Z_{VE1}$  according to

$$Z_{VE1}(\zeta_{link}, \zeta_{cube}, \xi) = Z_{cube}(\zeta_{cube}, \xi)^{L_0} \cdot Z_{link}(\zeta_{link})^{L_0V_3}. \quad (109)$$

The partition function  $Z_{cube}$  of the spacelike degrees of freedom reads

$$Z_{cube} = \int \prod_{x \in \Lambda_0^{(3)}} \left( d\nu(\Phi(x)) e^{-S^\circ(\Phi(x))} \prod_{\mu=1}^3 d\mu_H(U(x; \mu)) \right) \cdot \exp(-S_{cube}(U, \Phi)), \quad (110)$$

with  $\Lambda_0^{(3)}$  the 3-dimensional lattice and

$$S_{cube}(U, \Phi) = - \sum_{x \in \Lambda_0^{(3)}} \left\{ \sum_{\mu=1}^3 4\zeta_{cube} \phi_0(U(x; \mu)) + \xi \phi_0(\Phi(x)) + \sum_{\mu=1}^3 (2\kappa) \frac{1}{2} \text{tr}(\Phi(x)^\dagger U(x; \mu) \Phi(x + \hat{\mu})) \right\}, \quad (111)$$

while  $Z_{link}$  is an ultralocal one-link integral

$$Z_{link} = \int d\mu_H(U) \exp(-S_{link}(U)) \quad (112)$$

with

$$S_{link}(U) = 4\zeta_{link}\phi_0(U). \quad (113)$$

Expectation values  $\langle O \rangle_{cube}$ ,  $\langle O \rangle_{link}$ ,  $\langle O \rangle_{VE1}$  of observables  $O$  refer to  $Z_{cube}$ ,  $Z_{link}$  and  $Z_{VE1}$ , respectively. Minimization of the trial free energy density  $\tilde{f}(\zeta_{link}, \zeta_{cube}, \xi)$  in terms of these expectation values leads to three equations. The first one  $(\partial\tilde{f}/\partial\xi) = 0$  is solved by  $\xi = 0$  in the symmetric phase. The remaining two equations are given by

$$\begin{aligned} & \frac{\bar{\beta}}{4} \frac{\partial \widetilde{W}_{cube}^{1,2}}{\partial \zeta_{cube}} + \left[ \bar{\beta} (\langle \phi_0(U) \rangle_{cube})^3 + \frac{\bar{\beta}}{2} (\langle \phi_0(U) \rangle_{link})^2 \langle \phi_0(U) \rangle_{cube} - \zeta_{cube} \right] \\ & \cdot \frac{\partial}{\partial \zeta_{cube}} \langle \phi_0(U) \rangle_{cube} = 0 \end{aligned} \quad (114)$$

and

$$\left[ \frac{3\bar{\beta}}{2} (\langle \phi_0(U) \rangle_{cube})^2 \langle \phi_0(U) \rangle_{link} - \zeta_{link} \right] \cdot \frac{\partial}{\partial \zeta_{link}} \langle \phi_0(U) \rangle_{link} = 0. \quad (115)$$

Here we have used the shorthand notation

$$\begin{aligned} \langle \phi_0(U) \rangle_{cube} & \equiv \langle \phi_0(U(x; 1)) \rangle_{cube}, \\ \widetilde{W}_{cube}^{1,2} & \equiv \frac{1}{2} \langle \text{tr} U(x; 1) U(x + \hat{1}; 2) U(x + \hat{2}; 1)^{-1} U(x; 2)^{-1} \rangle_{cube} \\ & - (\langle \phi_0(U(x; 1)) \rangle_{cube})^4, \end{aligned} \quad (116)$$

with  $x \in \Lambda_0^{(3)}$ . In (116) we have used the lattice symmetries. Eq.s (114), (115) should be solved for  $\zeta_{link}$ ,  $\zeta_{cube}$ , and  $\xi$  as series in  $\kappa$ . The stability condition for the symmetric minimum at  $\xi = 0$  is given as

$$\begin{aligned} & 3\bar{\beta} \left. \frac{\partial^2 \widetilde{W}_{cube}^{1,2}}{\partial \xi^2} \right|_{\xi=0} \\ & + 12 \left[ \bar{\beta} (\langle \phi_0(U) \rangle_{cube})^3 + \frac{\bar{\beta}}{2} \langle \phi_0(U) \rangle_{cube} (\langle \phi_0(U) \rangle_{link})^2 - \zeta_{cube} \right] \\ & \cdot \left. \frac{\partial^2}{\partial \xi^2} \langle \phi_0(U) \rangle_{cube} \right|_{\xi=0} \\ & + \left[ (2\kappa) 2 \langle \phi_0(U) \rangle_{link} \left. \frac{\partial}{\partial \xi} \langle \phi_0(\Phi) \rangle_{cube} \right|_{\xi=0} - 1 \right] \cdot \left. \frac{\partial}{\partial \xi} \langle \phi_0(\Phi) \rangle_{cube} \right|_{\xi=0} \\ & < 0, \end{aligned} \quad (117)$$

with

$$\langle \phi_0(\Phi) \rangle_{cube} \equiv \langle \phi_0(\Phi(x)) \rangle_{cube}, \quad (118)$$

$x \in \Lambda_0^{(3)}$ . For an equality sign, (117) determines  $\kappa_{crit}$  order by order in the expansion.

Note the two type of expectation values  $\langle \cdot \rangle_{link}$ ,  $\langle \cdot \rangle_{cube}$  entering Eq.s (114), (115), (117). While the single link expectation values  $\langle \cdot \rangle_{link}$  can be evaluated exactly, the  $\langle \cdot \rangle_{cube}$ s must be approximated. The derivatives of  $\widetilde{W}_{cube}^{1,2}$  w.r.t.  $\zeta_{cube}$  or twice w.r.t.  $\xi$  induce up to 5-point functions in  $U$  and 6-point functions in four  $U$ s and two  $\Phi$ s. Because of the bad signal/noise ratio Monte Carlo calculations of such connected correlations would not be feasible. Therefore this is the place, where we use a DLCE to evaluate expectation values of the type  $\langle U \cdots U \Phi \cdots \Phi \rangle_{cube}$  (all internal and configuration space indices suppressed) order by order in  $\kappa$ . Clearly, also in this scheme the price is high. For example, the number of connected DLCE graphs contributing to order  $\kappa^4$  to a 4-point function of 2  $U$ s and 2  $\Phi$ s is about 100. Not all correlations in (114),(115),(117) appear in the form of susceptibilities. In a product of 4  $U$ s, for instance, the configuration space indices are fixed to the boundary of a plaquette. Such features must be noticed for calculating the graphical weights.

These remarks may indicate the complexity of the actual evaluation of Eq.s (114), (115), (117). Here we omit any further details on the list of contributing graphs and postpone them to [19]. Before we quote some results, we comment on further subtleties, when DLCEs are adapted to internal symmetries of the hopping term.

## 7.2 DLCEs for internal symmetries

In this section we focus on the (gauge) group  $SU(2)$ , since we are interested in applications to the electroweak phase transition, but it should be obvious, how one could proceed along the same lines for a group  $SU(N)$  with  $N > 2$ . In the development of the multiple-line graph theory in sections 3-5 we had assumed that  $\phi \in \mathbf{R}$ ,  $U \in \mathbf{R}$  to simplify the notation. In Eq.s (98) and (99) we had  $\Phi \in cU(2)$ ,  $U \in SU(2)$ . Let us write the hopping part of the action in the symmetrized form

$$S_{hop} = -\frac{1}{2} \sum_{x,y \in \Lambda_0} v(x,y) \frac{1}{2} \text{tr} \Phi(x)^\dagger U(x,y) \Phi(y), \quad (119)$$

with hopping parameter

$$v(x,y) = 2\kappa \sum_{\mu=0}^3 (\delta_{y,x+\hat{\mu}} + \delta_{y,x-\hat{\mu}}) \quad (120)$$

and

$$\begin{aligned} U(x, x + \hat{\mu}) &= U(x; \mu) \\ U(x + \hat{\mu}, x) &= U(x; \mu)^{-1} \quad , \quad \mu = 0, \dots, 3, \\ U(x, y) &= 0 \quad \text{otherwise} \end{aligned} \quad (121)$$

Using the parametrizations (98) and (99) we have

$$\frac{1}{2} \text{tr} \Phi(x)^\dagger U(x,y) \Phi(y) = \phi(x) \cdot \phi(y) U_0(x,y)$$

$$\begin{aligned}
& +\phi_0(y) \vec{\phi}(x) \cdot \vec{U}(x,y) - \phi_0(x) \vec{\phi}(y) \cdot \vec{U}(x,y) \\
& +\vec{\phi}(x) \times \vec{\phi}(y) \cdot \vec{U}(x,y).
\end{aligned} \tag{122}$$

Note that in the parametrization in terms of  $(\phi_0, \vec{\phi})$ s and  $(U_0, \vec{U})$ s the  $S^\circ$  part of the action is  $O(4)$  invariant, but  $S_{VE1}$  is only  $O(3)$  invariant for  $\zeta \neq 0$  or  $\xi \neq 0$ . Thus we have to distinguish between singlet (0) and triplet ( $s = 1, 2, 3$ ) indices in internal space.

Recall the generating equations (6) of the graphical expansion of a DLCE in which  $\langle \Phi(x)U(x,y)\Phi(y) \rangle$  had been expressed in terms of connected  $n$ -point functions,  $n = 1, 2, 3$ . Using the  $O(3)$  symmetry it follows from Eq. (122) that each derivative  $\partial/\partial I(x,y)$  now has to be replaced by the differential operator

$$L_{ab}(x,y) = \delta_{ab} \frac{\partial}{\partial I_0(x,y)} + \sum_{\gamma=1}^3 (\delta_{a,\gamma} \delta_{b,0} - \delta_{b,\gamma} \delta_{a,0} + \epsilon_{ab\gamma}) \frac{\partial}{\partial I_\gamma(x,y)}. \tag{123}$$

Latin indices run from 0 to 3, Greek indices from 1 to 3. Furthermore we have introduced the totally antisymmetric  $\epsilon$ -symbol which is zero if any of the three indices is zero and  $\epsilon_{123} = 1$ . This implies for instance for the one nonvanishing term at  $v = 0$  in Eq. (6) a substitution according to

$$W_{H(x)}W_{H(y)}W_{I(x,y)} \longrightarrow W_{H^a(x)}W_{H^b(y)}L_{ab}(x,y)W. \tag{124}$$

According to the graphical rules an  $n$ -line was generated by  $n$  iterated derivatives w.r.t.  $I_j, j \in 0, 1, 2, 3$ , evaluated at  $v = 0$ . These derivatives now have to be replaced by a multiple application of  $L$  yielding an  $n$ -line

$$\begin{array}{c}
\begin{array}{ccc}
& \text{---} & \\
a_1 & \text{---} & b_1 \\
& \text{---} & \\
x & \text{---} & y \\
a_2 & \text{---} & b_2 \\
& \vdots & \\
& \text{---} & \\
a_n & \text{---} & b_n
\end{array}
\end{array}
y = \sum_{\mu=0}^3 (\delta_{y,x+\hat{\mu}} + \delta_{y,x-\hat{\mu}}) (2\kappa)^n \left( \prod_{i=1}^n L_{a_i b_i} \right) W^1(I) \Big|_{I=0} \tag{125}$$

where the 1-link generating function  $W^1(I)$  is defined by

$$\exp W^1(I) = \frac{\int d\mu_H(U) \exp(4\zeta_{cube}\phi_0(U) + \sum_{a=0}^3 I_a \phi_a(U))}{\int d\mu_H(U) \exp(4\zeta_{cube}\phi_0(U))}. \tag{126}$$

For  $a_i = b_i = 1$  for all  $i \in 1, \dots, n$ ,  $n$  applications of  $L_{ab}$  to  $W^1$  reduce to  $\delta_{ab} \partial^n W^1 / \partial I^n |_{I=0}$ , but otherwise we get a complicated mixing of singlet and triplet terms.

To evaluate products of  $L$ s systematically, it is again quite convenient to manipulate graphical rather than analytic expressions. We represent one application of  $L_{ab}$  on  $W^1$  as shown in Fig. (11). Multiple applications of  $L_{ab}$  require an iteration of Fig. (11).

Twiddle lines are bare  $\phi$ -lines with a singlet index  $a = 0$ , crossed lines are bare  $\phi$ -lines with a triplet index  $a = 1, 2, 3$ . The arrow in the last term stands for the  $\epsilon_{ab\gamma}$  symbol in  $L_{ab}$ , its orientation reflects the order of indices  $ab\gamma$ .

Figure 11: Graphical representation of  $L_{ab}W^1$ . It provides the generating equation for the graphical computation of the internal symmetry factor of a multiple-line. It replaces Fig. 1(b) for  $I = H = 0$ ,  $v = 0$  and  $n = 1$ . For further explanations see the text.

This way one achieves a further graphical "decomposition" of an  $n$ -line into terms merely consisting of bare lines, from which the internal symmetry factors can be easily read off. For example a 2-line is further decomposed into 11 terms, a 3-line into 29 and a 4-line into 142. This may indicate that the number of decomposed contributions rapidly increases with the number  $n$  of bare lines collected to an  $n$ -line. In our actual calculations up to order  $\kappa^4$  the maximal number of internal lines was 4 and the highest multiple line was a 6-line with 4 internal and 2 external U-lines. Some of the results will be reported in the next section.

### 7.3 Some results

In Table 1 we compare results for  $\kappa_{crit}$  obtained for 2 values of  $\bar{\beta}$  and  $\lambda$  and various lattice volumes within three methods. The first line refers to a naive molecular field approximation with a partition function  $Z_{VE0}$  factorizing according to Eq. (108). Because of the complete factorization in space and time directions the ansatz keeps only a trivial volume dependence and is temperature independent by construction.

The second line refers to Monte Carlo simulations of the SU(2) Higgs model in four dimensions [15] for two lattice extensions  $L_0 = 2$  and 3.

The third line shows results of the DLCEs with the variational ansatz (VE1) presented in section 7.2. Again this ansatz is independent of  $L_0$  by construction, so that we get an identical result for  $L_0 = \infty$ . The values for  $\kappa_{crit}$  have been obtained by a linear regression in  $1/R^2$ ,  $R$  denoting the order in  $\kappa$  of the DLCE. For the regression we used the coefficients of  $\kappa^1$ ,  $\kappa^2$ ,  $\kappa^3$  and  $\kappa^4$ . The value of  $\kappa_{crit}$  at order  $\kappa^4$  was given by 0.1284 for  $\lambda = 5 \cdot 10^{-4}$  and  $\bar{\beta} = 8.0$ . Although the fourth order seems to be low for a series expansion, the agreement with the Monte Carlo results is not too surprising, if we remind the complexity of the expansion, which is manifest in the number of graphs contributing at fourth order to the various expectation values.

Furthermore, for otherwise fixed parameters, we see a decrease of  $\kappa_{crit}$  between the Monte Carlo and the DLCE results for increasing  $L_0$ . This is in qualitative agreement with the expectation.

Method	$\beta$	$\lambda$	lattice	$\kappa_{crit}$
Mean Field	8.0	$5.0 \cdot 10^{-4}$	$\infty^4$	0.12973
Monte Carlo	8.0	$5.0 \cdot 10^{-4}$	$2 \cdot 32 \cdot 32 \cdot 256$	0.12887(1)
VE1 & DLCE	8.0	$5.0 \cdot 10^{-4}$	$4 \cdot \infty^3$	0.1282(1)
Mean Field	8.15	$5.1 \cdot 10^{-4}$	$\infty^4$	0.12964
Monte Carlo	8.15	$5.1 \cdot 10^{-4}$	$3 \cdot 48 \cdot 48 \cdot 384$	0.12852(2)
VE1 & DLCE	8.15	$5.1 \cdot 10^{-4}$	$4 \cdot \infty^3$	0.1281(1)

Table 1: Results for  $\kappa_{crit}$  for 2 values of  $\bar{\beta}$  and  $\lambda$ , various lattice extensions, and 3 methods. The Monte Carlo results are taken from [15], the mean field and DLCE results, extrapolated to infinite order, from this paper. (The error in the DLCE results refers to the extrapolation of  $\kappa_{crit}$ .)

In Table 2 we compare results for  $\kappa_{crit}$ , to order  $\kappa^4$  (first column) and extrapolated to infinite order (with the same regression as explained above) (second column) for DLCEs with different variational estimates. The couplings are fixed, and  $L_0 = 4$ . VE1 refers to the first variational ansatz, also exposed in Table 1. The ansätze for the variational estimates VE2 and VE3 will be explained in detail in [19]. Here we only characterize them by their different factorization properties of the partition function.

Ansatz	$O(\kappa^4)$	extrapolated
VE1	0.1284	0.1282(1)
VE2	0.12958	0.12910(6)
VE3	0.12948	0.12934(7)

Table 2: Results for  $\kappa_{crit}$ , obtained in a DLCE to order  $\kappa^4$  (second column) and extrapolated to infinite order (third column) at  $\beta = 8.0$ ,  $\lambda = 5 \cdot 10^{-4}$ ,  $L_0 = 4$ . The ansätze VE1, VE2, VE3 refer to 3 variational estimates for the free energy of an SU(2) Higgs model. Their gap equations are solved with DLCE.

The partition function  $Z_{VE2}$  factorizes according to

$$Z_{VE2}(\zeta_{(0,string)}, \zeta_{(s,link)}, \xi) = Z_{(0,string)}(\zeta_{(0,string)}, \xi)^{V_3} \cdot Z_{(s,link)}(\zeta_{(s,link)})^{3L_0V_3}, \quad (127)$$

i.e., a product of a partition function  $Z_{(0,string)}$  that couples fields with hopping parameter terms along a string in time direction, and  $Z_{(s,link)}$ , a partition function for a single spatial link. While expectation values w.r.t.  $Z_{(s,link)}$  can be evaluated exactly (within the numerical accuracy), expectation values w.r.t.  $Z_{(0,string)}$  are

preferably evaluated with DLCE. This way they do depend on  $L_0$ , in principle they are sensitive to detect a temperature effect on  $\kappa_{crit}$ . So far the couplings along a string are only kept in time direction, while the spacelike directions are incorporated on a mean field level in  $Z_{(s,link)}$ .

The third variational ansatz VE3 therefore is chosen as a symmetrized version of VE2 in that the string now can extend in any of the 4 directions. Again we treat space- and timelike degrees of freedom differently, because we are interested in systems at finite temperature with temperature dependent coupling  $\kappa_{crit}$ . The number of variational parameters is larger, each of it depending on two indices telling us whether the parameter belongs to a single link action or to a string, and whether the string extends in temporal or spacelike directions.

For both versions VE2 and VE3 the actual  $L_0$  dependence ( $L_0 = 4, \infty$ ) lies outside the systematic error, if we expand the series to order  $\kappa^4$ . For  $L_0 = 4$  the fourth order is the minimal order in  $\kappa$  at which a finite temperature effect is visible in principle. (For the graphs it should be possible to wind at least once around the torus in 0-direction.) At  $O(\kappa^4)$  the part of graphs for which the lattice embedding is sensitive to  $L_0$  is about 1% of the total number of graphs. Such a small "signal/noise" ratio produces an effect in the 7th or 8th digit, outside the error of the  $O(10^{-4})$  because of the truncation of the DLCE series. By increasing the order of the expansion, finite-temperature effects will become more pronounced. For higher orders an algorithmic implementation of the proliferating graphs becomes unavoidable.

## 8 Summary and Conclusions

In this paper we have introduced a new expansion scheme for 3-point interactions or, more precisely, for point-link-point interactions. This scheme generalizes linked cluster expansions for 2-point interactions by including hopping parameter terms endowed with their own dynamics. In chapters 3-5 we have developed a multiple-line graph theory with an additional new type of multiple-line connectivity. We have introduced appropriate equivalence classes of graphs and discussed the issue of renormalization. The main building blocks for an algorithmic generation of graphs have been constructed. Because of the fast proliferation of graphs already at low orders in the expansion, a computer aided implementation becomes unavoidable, if one is interested in higher orders of the expansion than we have computed so far.

In chapter 6 we have indicated promising applications to spin glass systems. In particular we have identified the DLCE graphs contributing to the link-average  $[[\ln Z_\beta(U)]]$  of the spin free energy  $\ln Z_\beta(U)$ . In the past such quantities often were only accessible by means of the replica trick.

In section 7 we have outlined encouraging results for the transition line of the electroweak phase transition within the SU(2)-Higgs model. The results have been obtained by DLCEs applied to gap equations that follow from variational estimates

of the free energy. They are in good agreement with corresponding high precision Monte Carlo results. As we have seen, the main complications of DLCEs for SU(N) Higgs systems come from the internal symmetry structure of the hopping term. In a forthcoming paper we will demonstrate how one has to refine the graphical representation to calculate internal symmetry factors merely within a graphical expansion.

In conclusion, DLCEs are involved, but practicable, at least with computer aided generation of graphs. They provide an analytical tool to study systems in situations in which it has been impossible so far.

## Acknowledgment

We would like to thank Reimar Kühn (Heidelberg) for pointing out to us ref.s [12]-[14].

## References

- [1] M. Wortis, "Linked cluster expansion", in Phase transition and critical phenomena, vol.3, eds. C. Domb and M.S. Green (Academic Press,London 1974).
- [2] C. Itzykson, J.-M. Drouffe, "Statistical field theory", vol.2, Cambridge University Press, 1989.
- [3] A.J. Guttmann, "Asymptotic analysis of Power-Series Expansions", in Phase transition and critical phenomena, vol.13, eds. C. Domb and J.L. Lebowitz (Academic Press).
- [4] M. Lüscher and P. Weisz, Nucl. Phys. **B300**[FS22] (1988) 325.
- [5] T. Reisz, Nucl. Phys. **B450** (1995) 569.
- [6] T. Reisz, Phys. Lett. **360B** (1995) 77.
- [7] M. Campostrini, A. Pelissetto, P. Rossi and E. Vicari, Nucl. Phys. **B459** (1996) 207.
- [8] S. Zinn, S.-N. Lai and M. E. Fisher, Phys. Rev. **E54** (1996) 1176.
- [9] P. Butera and N. Comi, Phys. Rev. **E55** (1997) 6391.
- [10] H. Meyer-Ortmanns and T. Reisz, Jour. Stat. Phys. **87** (1997) 755.
- [11] A. Pordt and T. Reisz, Int. Jour. Mod. Phys. **A12** (1997) 3739-3757.
- [12] D. Sherrington and S. Kirkpatrick, Phys. Rev. Lett **35** (1975) 1972.
- [13] V. Dotsenko, S. Franz and M. Mézard, J. Phys. **A27** (1994) 2351.



- [14] R. W. Penney, A. C. C. Coolen, and D. Sherrington, *J. Phys. A: Math. Gen.* **26** (1993) 3681. A. C. C. Coolen, R. W. Penney, and D. Sherrington, *Phys. Rev.* **B48** (1993) 16116.
- [15] Z. Fodor, J. Hein, K. Jansen, A. Jaster and I. Montvay, *Nucl. Phys.* **B439** (1995)147.
- [16] T. Reisz, “Hopping Parameter Series Construction for Models with Nontrivial Vacuum”, hep-lat/9802023, submitted to *Nucl. Phys. B*.
- [17] K. H. Fischer and J. A. Hertz, “Spin Glasses”, Cambridge University Press, Cambridge 1991.
- [18] J. Zinn-Justin, “Quantum Field Theory and Critical Phenomena”, 3rd Edition, Oxford Science Publication, Clarendon Press, Oxford 1996.
- [19] H. Meyer-Ortmanns and T. Reisz, in preparation.